Marcelo Porto Becker

# A Mean-Field Method for Generic Conductance-Based Integrate-and-Fire Neurons with Finite Timescales

Porto Alegre

July, 2022

Marcelo Porto Becker

# A Mean-Field Method for Generic Conductance-Based Integrate-and-Fire Neurons with Finite Timescales

Dissertation conducted under the supervision of Professor Dr. Marco Aurélio Pires Idiart and presented to the Institute of Physics of UFRGS in partial fulfillment of the requirements to obtain the title of Master in Physics

Universidade Federal do Rio Grande do Sul – UFRGS

Instituto de Física

Programa de Pós-Graduação

Supervisor: Marco Aurélio Pires Idiart

Porto Alegre

July, 2022

Marcelo Porto Becker
A Mean-Field Method for Generic Conductance-Based Integrate-and-Fire Neurons with Finite Timescales/ Marcelo Porto Becker. – Porto Alegre, July, 2022-
66 p. : il. (algumas color.) ; 30 cm.

Supervisor: Marco Aurélio Pires Idiart

Dissertação (Mestrado) – Universidade Federal do Rio Grande do Sul – UFRGS
Instituto de Física
Programa de Pós-Graduação, July, 2022.

1. Palavra-chave1. 2. Palavra-chave2. I. Orientador. II. Universidade xxx. III. Faculdade de xxx. IV. Título

CDU 02:141:005.7

# Acknowledgements

Primeiramente, agradeço ao meu orientador Marco Idiart pelas discussões e por confiar no caminho que segui. Mas principalmente, agradeço por ter aguentado eu ter trazido um monte de cálculos no meio do projeto e mudado o rumo do mesmo.

Agradeço a minha mãe pelo apoio incondicional e por fornecer a estrutura necessária durante toda minha formação. Não poderia ter alguém melhor.

Agradeço também a minha namorada por ser uma grande companheira, por ajudar a tornar o processo mais leve e por superestimar minha inteligência.

Por fim, agradeço aos meus colegas de grupo, por aguentarem ver minha cara em todas as reuniões virtuais que compartilhamos.

*"Those swirls in the cream mixing into the coffee? That's us.*
*Ephemeral patterns of complexity, riding a wave of increasing*
*entropy from simple beginnings to a simple end. We should enjoy the ride."*
*(Sean Carroll, The Big Picture:*
*On the Origins of Life, Meaning, and the Universe Itself)*

# Resumo

A construção de funções de transferência na neurociência teórica desempenha um importante papel na determinação do comportamento das taxas de disparos de neurônios em redes. Elas podem ser obtidas por uma variedade de métodos de ajuste onde a relevância dos parâmetros biológicos não são sempre claros. Entretanto, esses tipos de funções podem ser obtidos para entradas estacionárias pelo uso de métodos de campo médio, sem o ajuste de parâmetros livres. Para um neurônio simples de integração e disparo baseado em correntes, onde o ruído é branco e aditivo, a função de transferência foi obtida por Amit e Brunel através da construção de uma equação de Fokker-Planck. Varias extensões para esse método foram introduzidas para dar conta de diferentes tipos de neurônios, mas o problema de um ruído genérico, colorido e multiplicativo ainda não foi atacado. Aqui nós propomos uma solução a esse problema.

Para fazer isso, nos reduzimos o sistema estocástico que resulta da aplicação da aproximação de difusão a uma equação de Langevin unidimensional. Essa equação de Langevin é então colorida e não pode produzir uma equação de Fokker-Planck exata. Nos então usamos uma extensão para a teoria de Fox para construir uma equação de Fokker-Planck efetiva com múltiplas fontes de ruído colorido e multiplicativo. A taxa de disparos foi então calculada numericamente partindo da Fokker-Planck estacionária resultante. A solução foi capaz de reproduzir o comportamento da função de transferência dos neurônios simulados em uma grande gamma de parâmetros. O método também pode ser facilmente estendido para considerar diferentes fontes de ruído com diferentes termos multiplicativos, e a princípio pode ser utilizado em outros tipos de problemas.

**Palavras-chaves**: neurociência. campo médio. integração e disparo. função de transferência.

# Abstract

The construction of transfer functions in theoretical neuroscience plays an important role in determining the behavior of the spiking rate of neurons in networks. They can be obtained by a variety of fitting methods where the biological relevance of the parameters is not always clear. However, this type of function can be obtained for stationary inputs by the use of mean-field methods, without adjustment of free parameters. For a simple current base integrate and fire neuron, where the noise is white and addictive, the transfer function was obtained by Amit and Brunel through the construction of a Fokker-Planck equation. Several extensions to this method were introduced to account for different types of neurons, but the problem of a generic colored multiplicative noise has yet to be tackled. Here we proposed a solution to this problem.

To do this, we reduced the stochastic system resulting from the application of the diffusion approximation to a one dimensional Langevin equation. This Langevin equation is therefore colored and cannot produce a exact Fokker-Planck equation. We then used an extension to the Fox theory to build an effective Fokker-Planck equation with the multiple sources of colored and multiplicative noise. The firing rate was then calculated numerically from the resulting stationary Fokker-Planck. The solution was able to reproduce the transfer function behavior of the simulated neurons in a wide range of parameters. The method is also easily extendable to account for different sources of noise with different multiplicative terms, and in principle can be used in other types of problems.

**Key-words**: neuroscience. mean-field. integrate and fire. transfer function.

# List of Figures

# List of Tables

# Contents

# 1 Introduction

The brain is a complex system that organizes itself in structures that can range from fine-scale details (YOSHIMURA; CALLAWAY, 2005), to large-scale arrangements involving large portions of the cortex (KOZIOL et al., 2014). These structures are invariably composed of neurons and other supportive cells that interact with each other in complex ways (VOGELS; RAJAN; ABBOTT, 2005). This whole range of scales that the brain operates can make it difficult to navigate. For example, experimentally we can probe individual neurons with great time and spatial resolutions but probing single cells don't give much information about the collective behaviors of the system. Microelectrode arrays can provide multiple sources of measurement, but spatial resolution is lost since the microelectrodes capture signals from all around the sensors (OBIEN et al., 2014). On the other end of the spectrum, functional magnetic resonance imaging (fMRI) can provide large-scale information about the activity, but have a low temporal and spatial resolution (GLOVER, 2011).

To bridge these multiple scales problems, theoretical models and frameworks are of great relevance. Indeed, these kinds of problems are not new to physics and especially to condensed matter physics, where collections of atoms give rise to new behaviors that can depend on small and large scales of the system (STANLEY, 1971)(YEOMANS, 1992). A plethora of methods to treat this types of problems was developed by condensed matter physics and later co-opted by theoretical neuroscientists. One of these methods is known generically by the name mean-field theories and encompasses a large family of procedures. It was initially created by Curie and Weiss with the intent to describe phase transitions in magnetic systems (STANLEY, 1971)(YEOMANS, 1992)(WEISS, 1907), and later expanded into a wide range of approaches that are used in a diversity of fields.

In neuroscience, it can be used to create firing rate models (also sometimes described as transfer functions) from the description of spiking neurons models, for example (CAMERA, 2021)(BRUNEL; SERGI, 1998)(BRESSLOFF, 2011)(OSTOJIC; BRUNEL, 2011), bridging the gap between the microscopic and the mesoscopic description. The mean-field in those cases goes beyond the typical substitution of the complex interaction input by its mean. Since neurons can generate spikes even when the mean input is below its threshold, it is necessary to add also a fluctuating part. Therefore, mean-field theories in spiking neurons behave similarly to models of Brownian motion.

For some integrate and fire neuron models, the resulting Brownian motion description can present itself with temporal correlation in the noise (colored noise) and also nonlinear multiplicative terms. These kind of motions presents difficulties in the exact

treatment and the derivation of the resulting firing rate. The present work provides a method to construct firing rate models from generic conductance base integrate and fire neurons, which can present colored and multiplicative noise in its Brownian description. In the next subsections we will provide some basic informations for the comprehension of the main results.

## 1.1 Neurons and Networks

In this subsection, we will briefly revise the physiology of the neuron and synapses. More detailed discussions about the topic can be seen in books like (PURVES et al., 2019) for a biological focus, or (IZHIKEVICH, 2007) and (DAYAN; ABBOTT, 2005) for a mathematical look.

Neurons are highly specialized cells responsible for the storage and transmission of information. This storage and transmission are done by changes in the electrical properties of the membrane of the cell. Specifically, we are talking about the difference in the electrical potential between the interior and the exterior of the cell. This difference is generated by different concentrations of ions on both sides of the membrane generated by ionic pumps that pump ions through the membrane, using energy in the process. The most important of these pumps is the sodium-potassium pump, which moves 3 sodium ions to the exterior of the cell and 2 potassium ions to the interior, generating a net flux of positive charges to the exterior.

Another source of charge unbalance is the composition of ionic channels of the cell membrane. Ionic channels can selectively allow the passage of specific ions, generating a passive current. Some channels are permanently open, such as the leak channels that allow the passage of potassium ions. Others need to be activated by some form of a signal, such as the binding of a chemical or the depolarization of the membrane patch that it is embedded in.

For every ion, we can calculate the equilibrium potential resulting from its net flux. This is done by the Nernst equation, which takes into consideration the flux given by the diffusion of the ion and the flux resulting from the electrical potential itself. The form of the equation is

$$V_{ion} = \frac{RT}{zF} \ln \frac{[ion]_{out}}{[ion]_{in}}\,, \tag{1.1.0.1}$$

where $R$ is the universal gas constant, $T$ is the temperature in Kelvin, $z$ is the valence number of the ion and $F$ is the Faraday constant. From the simple Ohm's law we can get the associated current for the ion

$$I_{ion} = g_{ion}(V - V_{ion})\,, \tag{1.1.0.2}$$

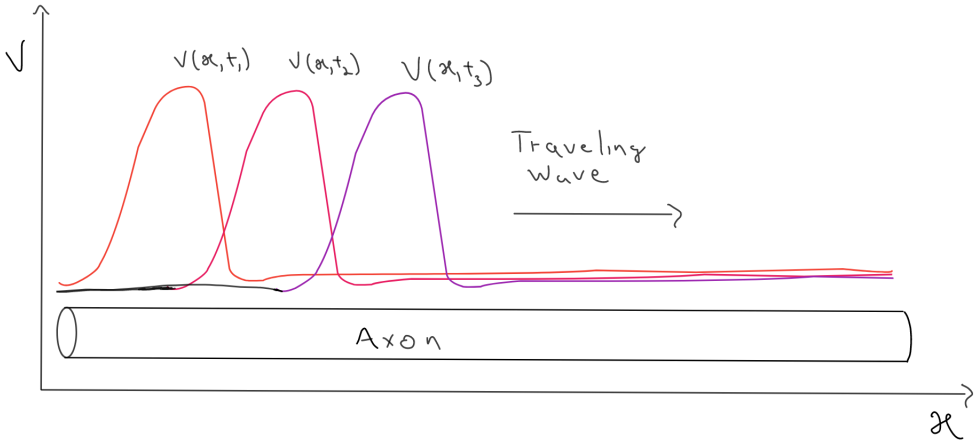


Figure 1 – Schematics of a traveling pulse resulting from the action potential process.

where $g_{ion}$ is the conductance for the ion. The resulting rest potential can then be inferred by taking the weighted average of all the ionic contributions. This is mostly given by

$$V_{rest} = \frac{g_{K^+}V_{K^+} + g_{Na^+}V_{Na^+} + g_{Ca^{2+}}V_{Ca^{2+}} + g_{Cl^-}V_{Cl^-}}{g_{K^+} + g_{Na^+} + g_{Ca^{2+}} + g_{Cl^-}} . \tag{1.1.0.3}$$

As already mentioned, some of the channels can be activated and deactivated by the value of the membrane potential at the local membrane patch. These channels are responsible for the signal emission process known as the action potential. To be precise, two types of voltage-dependent channels contribute to the generation of action potentials: sodium transient channels and persistent potassium current channels. Both channels are activated when the potential reaches a certain threshold value. The sodium transient channels activate slightly faster than the potassium ones and produce a depolarization. This generates more depolarization in the vicinity of the channel and triggers more voltage-dependent channels to activate. The signal then propagates through the neuron. The potassium persistent channels can then repolarize the membrane patch by allowing potassium ions to flow outside the cell. The traveling pulse resulting from this process is schematized in figure 1. After an action potential, the cell enters a brief period where it can't emit another spike. This period is called the absolute refractory period and can last a few milliseconds.

Neurons also receive inputs mostly by chemical signals. Those come in the form of small molecules that are liberated in the extracellular medium between the contact point of both neurons, the synaptic gap. In this directional contact, the receiving neuron (the postsynaptic neuron) has channels that open when the specific molecule liberated in the

gap binds to it. These channels then open and produces changes in the membrane potential that passively propagates through the neuron. The nature of these changes depends on the ion selectivity of the channel. The channel can be excitatory, producing depolarization of the neuron; or inhibitory, if it produces a hyperpolarization. In general, it is supposed that a neuron can make only excitatory or inhibitory synapses (Dale's principle). In this sense, a neuron can be considered excitatory or inhibitory.

The most common receptor-neurotransmitter pair in the cortex is the AMPA-glutamate pair. The AMPA receptor ($\alpha$-amino-3-hydroxy-5methyl-4-isoxazolepropionic acid receptor) is a tetrameric (composed of four subunits) channel that allows the passage of both potassium and sodium ions. The equilibrium potential of this channel is greater than the resting potential and therefore it produces a depolarizing current. AMPA receptors are generally fast-acting, with a response time of around a millisecond. However, slow AMPA receptors were also found in the hippocampus, staying active for about half a second (PAMPALONI et al., 2021). Another common glutamate receptor is the NMDA receptor (N-methyl-D-aspartate), which is permeable by sodium ions and also calcium. It is also an excitatory channel since its reversal potential is also greater than the resting potential. However, the opening of the NMDA channels depends also on the membrane potential at the moment of the glutamate binding. This occurs because in the structure of the receptor there are magnesium ions that block the passage of the sodium and calcium ions when the membrane is at rest. When the membrane is depolarized, those magnesium ions are dislocated from the channel, allowing current to flow (figure 2). NMDA receptors have slow dynamics, acting on the order of a hundred milliseconds.

The typical inhibitory receptor in the cortex is the GABA receptor (gamma-aminobutyric acid). There are three distinct types of GABA receptors that have different compositions and different functions. $GABA_A$ and $GABA_C$ behaves as a typical ionic channels, allowing the passage of chlorine ions, which have an equilibrium potential smaller than the resting potential (in most cases). $GABA_B$ is what we call a metabotropic receptor, which is a receptor that initiate metabolic changes in the neuron via G protein.

Neurons have distinct physical structures. Even though there is a great zoo of types of neurons, most of them can be divided into three parts: the dendrites, the soma, and the axon (figure 3). The dendrites have an arboreal shape and are specialized in the reception of signals from other neurons. Most of the synapses are located in this region and as a consequence, most of the synaptic receptors. The soma is the cell body, where most cellular processes occur. Some synapses can also be located in the soma, but to a lesser degree. The axon is the long projection that can ramify in its extremities. It functions as the signal emitter and has a large concentration of voltage-dependent channels. They make connections with other neurons and liberate the neurotransmitters in their synaptic end that communicate with the other neurons. In this way, the integration of

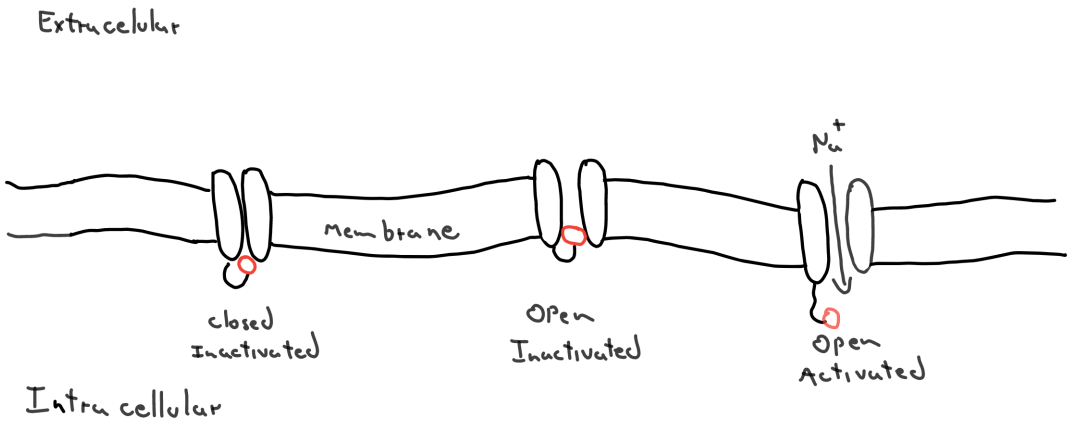


Figure 2 – Dynamics of the NMDA opening and closing.

the signal and firing "decision" is done in the intersection between the soma and the axon, a region sometimes called the axon hillock. Even though neurons have this rich architecture, most theoretical works reduce this structure to a single point-like structure, that integrates signals and emits spikes. This will be the framework adopted here since a cable-like treatment can significantly complicate the mathematical modeling (NIEBUR, 2008)(DAYAN; ABBOTT, 2005).

## 1.2 The Neuron as a Transfer Function

Neuron alone exhibits highly complex behaviors (MILLER, 1999)(NOBUKAWA et al., 2015). This complex vocabulary can then be concatenated and built upon to generate even more diverse and rich dynamics. However, not every detail is important for the description of every phenomenon. For example, memory models can rely on precise spike timings and dynamics to codify the stimulus presented (HAHNLOSER; KOZHEVNIKOV; FEE, 2002)(BUONOMANO; MAASS, 2009)(LAJE; BUONOMANO, 2013). This kind of code, sometimes called spike-timing code, is also important for coincidence detection in the auditory brainstem of mammals and birds (AGMON-SNIR; CARR; RINZEL, 1998). Their description requires more detailed information on the time course of the neuronal dynamics and therefore requires a more realistic model for the neural behavior. In other cases it is only necessary to know the firing rate evolution of the neuron, that is, we only

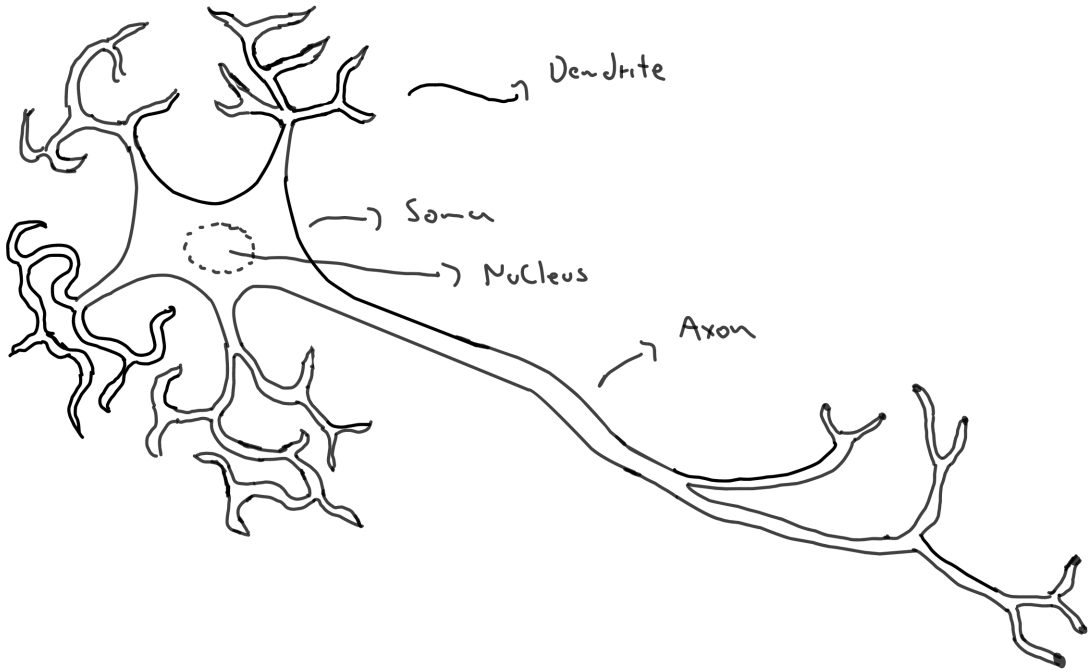


Figure 3 – Diagram of a stereotypical neuron.

need to know the time average of one of its dynamical properties. This is the case when we are talking about rate codes. Experimentally, rate codes were first discovered by inferring the stimulus from the readout of the firing rate in sensory neurons (ADRIAN, 1928). It became a well-established memory model and can account for some descriptions of working memory (MOLTER; COLLIAUX; YAMAGUCHI, 2008) and long-term memory (LUBOEINSKI; TETZLAFF, 2022) for example. In general, information extraction from a single neuron rate code is slow, since it is needed time to average the spikes to good precision. A way to circumvent this problem is to take the average of a population of weakly correlated neurons with similar functions instead of averaging single neurons over time. This way of tackling the problem correlates with the organization of the cortex, where a large number of neurons are arranged into columns where the function of its constituents is similar (MOUNTCASTLE, 1997). Therefore, the firing rate transfer functions can describe neurons to a good approximation when we are dealing with a mesoscopic level of interactions.

The most straightforward way to obtain the firing rate of a population of neurons is to simulate individual neurons as spiking neurons and then take the temporal or populational average of the spikes (figure 4). This process comes with its difficulties. The act of simulating networks of spiking neurons can be computationally expensive, and as the size of the network grows, the time necessary for simulating can grow much faster then the size. Not only that, but exploration of the parameter space of the neuron can become

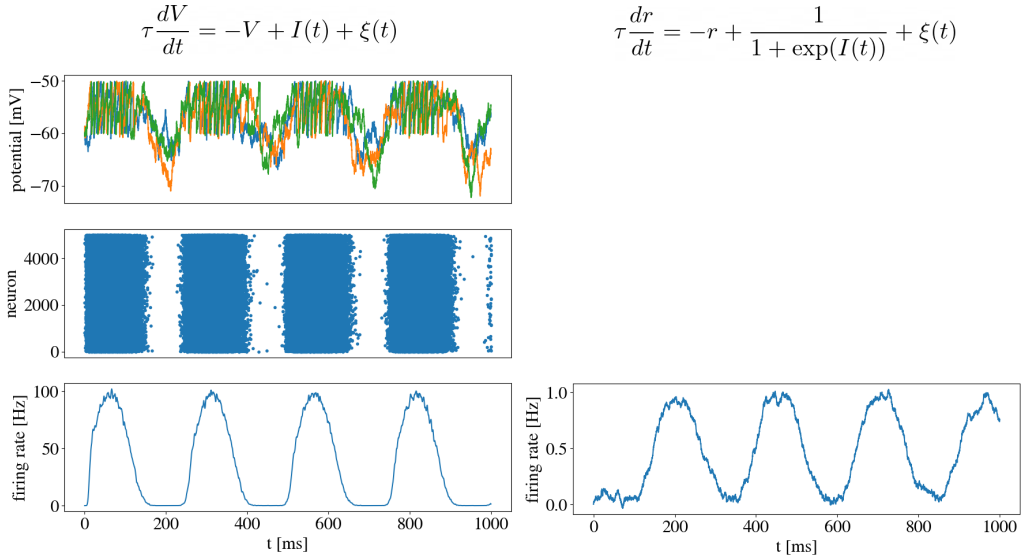


Figure 4 – Extracting the firing rate of a population of spiking neurons versus a phenomenological firing rate model. In the integrate and fire model, we simulate the potential of 5000 non-interacting neurons, plotting the potential for three of them, the spiking time, and the averaged firing rate. Both neurons receive a oscillatory current plus a noise. No attempt was made to make the dynamics equivalent.

unwieldy, since the parameter space is large.

Another way to treat this kind of system is to start with a form of phenomenological rate model (ERMENTROUT, 1998)(GERSTNER et al., 2014). They can be made to describe the firing rate evolution of a single neuron or of a whole population in what is called a neural mass model (figure 4). In general, this type of model is written as a set of differential equations where the functions to be solved are the firing rates of the neurons or the populations of neurons. The parameters in these models don't have an explicit relation to physiological parameters and encapsulate a variety of properties. Therefore, when necessary to connect experiment with the model, fitting procedures are needed make this connections. The great advantage of these models is how mathematically malleable and tractable they are. They can serve as ways to study phenomenons like phase transitions, network oscillations, attractor dynamics, and many more (ERMENTROUT, 1998).

There is, however, a way to bridge the gap between those two rate descriptions. That is, there is a way to construct a firing rate model that carries on the parameters of the spiking neuron and the input statistics. One way to do this is with the help of mean-field theories. The way the method proceeds is generally the following. We first suppose that the neuron receives input in the form of large population of neurons, each contributing with only a small change in the potential. This population is divided into groups of similar neurons and the resulting input from each of these groups is substituted by its mean and, generally, a fluctuating part. The fluctuating appears in contrast with

traditional mean-field theories in condensed matter physics because spikes in neurons can also be driven by this fluctuations. Since the relevant part for the rate description is the spikes, those fluctuations can be relevant contributors. The resulting equation after this procedure can be transformed into a equation on the probability of finding the system in a small interval of membrane potential, and this probability can be used to calculate the firing rate. We will detail the procedure in the next section, however, we can see how it brings the physiological parameters of the spiking neuron model to the rate model, making the fitting part unnecessary.

## 1.3 From Spiking Neurons to Rate Transfer Functions

We can trace back the idea of a mean-field approach to spiking neurons to the work of Gerstein and Mandelbrot (GERSTEIN; MANDELBROT, 1964). In their work, they noted that a great number of properties from the distribution of spikes of different neurons measured experimentally can be reproduced by a Brownian process with drift. Even though the form of the process was imposed as a solution, it can be shown that this kind of stochastic equation results from a mean-field treatment of the spiking neuron model known as the perfect integrate-and-fire neuron.

The first paper that brought up the approach used in the present work was the seminal paper by Amit and Brunel (AMIT; BRUNEL, 1997). Their method relies on constructing a Fokker-Planck equation that describes the probability distribution of the potential as a function of time. With this, it is possible to get a stationary transfer function by calculating the mean first passage time of the process. Since this method and some of the results are important to this work, we will lay out some of the derivations here. A detailed and didactic exposition can also be found in (FENG, 2003).

We start by exposing the neuron model from which we wish to extract the transfer function. The model is the current-based leaky integrate and fire neuron, written as

$$\tau \frac{dV}{dt} = (E_L - V) + \sum_{j,k} w_j \delta(t - t_j^k)\,, \tag{1.3.0.1}$$

where $\tau$ is the membrane time-constant, $V$ is the membrane potential, $E_L$ is the equilibrium potential, $w_j$ is the synaptic weight of $j$ synapse, $t_j^k$ is the time of the $k$-spike of neuron $j$ and $\delta()$ is the Dirac delta function. Suppose the sum accounts for two populations, an excitatory with $K_E$ neurons with firing rate $\nu_E$ and weight $w_E$, and an inhibitory one with $K_I$ neurons with rate $\nu_I$ and weight $w_I$. Also, suppose that both populations fire as a Poisson process. When the total number of input neurons is large and the synaptic weights are small, we can use the diffusion approximation, which substitutes the Poisson process with a Gaussian white noise with the same mean and variance, that is,

$$\tau \frac{dV}{dt} = (\mu - V) + \sigma_V \xi(t)\,, \tag{1.3.0.2}$$

where $\mu$ is the mean potential given by

$$\mu = E_L + K_E w_E \nu_E - K_I w_I \nu_I \,, \tag{1.3.0.3}$$

$\sigma_V$ is the standard deviation

$$\sigma_V^2 = K_E w_E^2 \nu_E + K_I w_I^2 \nu_I \,, \tag{1.3.0.4}$$

and $\xi$ is a Gaussian white noise with zero mean and unity variance. This is a standard Langevin equation that describes a stochastic process with a restoring force. Since the process is stochastic, the description of the potential is the given in terms of the probability distribution of $V$. A Fokker-Planck equation can then be obtained from the Langevin (RISKEN; FRANK, 2012):

$$\frac{\partial P(V,t)}{\partial t} = \frac{\partial}{\partial V}\left[\frac{(V-\mu)}{\tau} P(V,t)\right] + \frac{\sigma_V^2}{2\tau}\frac{\partial^2 P(V,t)}{\partial V^2} \,. \tag{1.3.0.5}$$

The Fokker-Planck can be used to calculate the stationary probability distribution of the potential as well as statistics of the spiking time, like the mean firing rate. Time-dependent analysis can also be done in some situations (Nicolas Brunel; Vincent Hakim, 1999)(BRUNEL et al., 2001)(FOURCAUD-TROCMÉ et al., 2003). Since their interest was in stationary properties, the time derivative is taken to be zero. The influence of the threshold, the reset potential, and the refractory period come in the form of boundary conditions. In fact, we have an absorbing wall at the threshold value, where the absorbed probabilities are reintroduced at the reset potential after passing the refractory period. It is also noted that the firing rate is the same as the probability current passing through the threshold. Applying these conditions to the Fokker-Planck results in the linear ODE

$$\frac{\partial}{\partial V}\left[\frac{(V-\mu)}{\tau} P_s\right] + \frac{\sigma_V^2}{2\tau}\frac{\partial^2 P_s}{\partial V^2} = -\nu\delta(V - V_r) \,, \tag{1.3.0.6}$$

where $P_s$ is the stationary probability distribution, $\nu$ is the firing rate, and $V_r$ is the reset potential. Solving this linear ODE with the appropriate boundary conditions gives the expression for the stationary distribution

$$P_s(V) = \frac{2\nu\tau}{\sigma_V} \exp\left(-\frac{(V-\mu)^2}{\sigma_V^2}\right) \int_{\frac{V-\mu}{\sigma_V}}^{\frac{\theta-\mu}{\sigma_V}} \Theta\left(x - \frac{V_r - \mu}{\sigma_V}\right) e^{x^2} dx \,, \tag{1.3.0.7}$$

where $\theta$ is the threshold value and $\Theta()$ is the Heaviside function. With the help of the normalization condition

$$\int_{-\infty}^{\theta} P_s(V) dV + \nu\tau_r = 1 \,, \tag{1.3.0.8}$$

we finally get the transfer function

$$\frac{1}{\nu} = \tau_r + \tau\sqrt{\pi} \int_{\frac{V_r-\mu}{\sigma_V}}^{\frac{\theta-\mu}{\sigma_V}} e^{x^2}(1 + \mathrm{erf}(x)) dx \,, \tag{1.3.0.9}$$

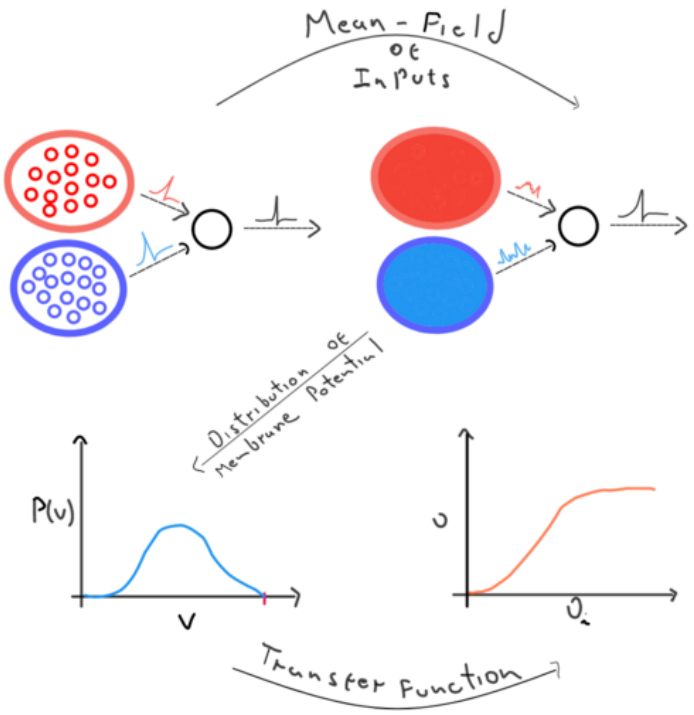


Figure 5 – Schematics of the Fokker-Planck mean-field approach. We start with a neuron receiving inputs from populations of similar neurons, here described by red and blue circles. A mean-field is taken from the inputs for each population, converting them into a Gaussian process. From the neuron receiving Gaussian inputs, we can extract the probability distribution of the potential using a Fokker-Planck equation. It is then possible to calculate the transfer function of the neuron.

with $\tau_r$ the refractory period. We schematized the procedure in figure

This procedure set the ground for the treatment of a variety of other models with different levels of complexity. The first extension that we can talk about is the addition of synaptic filtering in the current (BRUNEL; SERGI, 1998). This makes the synaptic inputs smooth but adds another dimension to the system. The multidimensional problem was then solved by constructing a Fokker-Planck of the distribution in the potential and current and then extracting the probability flux through the threshold line barrier. The result was a correction to the (1.3.0.9) that to a first approximation equates to a change in the threshold of the neuron.

Conductance-based models where the current is of the form $g_i(t)(E_i - V)$ and $g_i(t)$ are exponentially decaying pulses were dealt with in the approximation of instantaneous pulses (RICHARDSON, 2004). The model resulted in a one-dimensional multiplicative Langevin that can be used to generate a Fokker-Planck and then solved for the firing rate. It is also possible to get rid of the multiplicative term by using an approximation that substitutes the membrane potential in these terms with its stationary value (RICHARD-

SON; GERSTNER, 2005)(SANZENI; HISTED; BRUNEL, 2020). This approximation is called the effective time-constant approximation and we will talk about it a little bit more in the methods section.

Nonlinear terms in the leaky part of the integrate-and-fire models were also dealt with in this mean-field approach. The mean-field solution to the quadratic integrate-and-fire was found by Brunel and Latham (BRUNEL; LATHAM, 2003). The numerical solution of the exponential integrate-and-fire was constructed by Richardson, for example (RICHARDSON, 2007).

Generic time correlation were tackled for the perfect integrate and fire neuron, which doesn't have a leaky term (SCHWALGER; DROSTE; LINDNER, 2015). This correlations were treated by a process known as Markovian embedding that projects those noises into a multivariate Ornstein-Uhlenbeck process. In this way, the multivariate Fokker-Planck was solved in the small noise regime.

All of this leads us to a question: is it possible to construct a Fokker-Planck equation from a generic conductance-based integrate-and-fire neuron? That is, is it possible to arrive at a differential equation of the probability distribution of the potential from a Langevin with generic nonlinearities and colored noise? Is it also possible to extract the transfer function for a large range of parameters and time correlations? In a attempt to solve those problems, we looked at a different approach to construct a Fokker-Planck equation. That is the main focus of the current work.

## 1.4 Objectives

- Develop a mean-field approach to construct the transfer function of generic conductance-based integrate-and-fire neurons.
- Test the method for three different neuron models, increasing the complexity:
    1. A simple conductance-based integrate-and-fire neuron;
    2. A conductance-based integrate-and-fire neuron with interpolated fast and slow excitatory currents
    3. A conductance-based integrate-and-fire neuron with AMPA and nonlinear NMDA channels.

# 2 Methods

## 2.1 Model

We studied the behavior of a point like generic leaky integrate-and-fire (IF) neuron with conductance-based input embedded in a network of similar units. The neuron is described by the membrane potential $V$ that follows the differential equation

$$\tau_L \frac{dV}{dt} = -(V - E_L) - \sum_i g_i(t) s_i(V)(V - E_i) \tag{2.1.0.1}$$

where $\tau_L$ is the membrane time constant, $E_L$ is the resting potential, $E_i$ is the reversal potential of the corresponding channel $i$, and $s_i(V)$ is a modulating function that can depend on $V$. It is important to note that the addition of a nonlinear term $\psi(V)$ to the equation is possible in principle, although we will not deal with this case here. The conductances $g_i(t)$ behave as linear filters of the input signal. Specifically, we have

$$\tau_i \frac{dg_i}{dt} = -g_i + \sum_{j,k} w_i \delta(t - t_j^k) \tag{2.1.0.2}$$

The summation here is performed over all pre-synaptic sites $j$ and all spikes $k$ emitted in that site. $w_i$ is the synaptic weight which is kept the same for all neurons belonging to the same population.

The membrane potential $V$ evolves according to (2.1.0.1) until it reaches the threshold $\theta$, when it emits a spike. The potential is then reset to $V_r$ and after the reset, the membrane potential is not updated for the extent of the refractory interval $\tau_r$.

## 2.2 Mean-field analysis

### 2.2.1 Conductance

As a starting point, we suppose that the neuron receives inputs from separate populations of neurons corresponding to the different channels, each of them making $K_i$ connections. We assume that the inputs from each population come from Poisson rate neurons with fixed rate $\nu$. Considering a large number of connections in the system ($K_i \gg 1$) and a small connection weight ($w_i \ll 1$) we can make use of the diffusion approximation (AMIT; BRUNEL, 1997)(FENG, 2003). This approximation consists in changing the discontinuous nature of the spike input by a continuous white noise. It is similar to the treatment of a Brownian motion in one dimension, where the bumps of

fluid particles into the larger one are taken to be infinitesimally small. With this, equation (2.1.0.2) become

$$\tau_i \frac{dg_i}{dt} = -g_i + \mu_i + \sqrt{\tau_i}\sigma_i \xi_i(t) \tag{2.2.1.1}$$

where

$$\mu_i = w_i K_i \nu \tau_i \tag{2.2.1.2}$$

$$\sigma_i^2 = w_i^2 K_i \nu \tau_i \tag{2.2.1.3}$$

and the noise terms are uncorrelated Gaussian white noise with mean zero and unit variance:

$$\langle \xi_i(t) \rangle = 0 \qquad \langle \xi_i(t)\xi_i(t') \rangle = \delta(t - t')$$

$$\langle \xi_i(t)\xi_j(t') \rangle = 0 \quad \text{for } i \neq j$$

In the limit $t \gg \tau_i$, the solution of (2.2.1.1) is

$$g_i(t) = \mu_i + \frac{\sigma_i}{\sqrt{\tau_i}} \int_0^t e^{-\frac{T}{\tau_i}} \xi_i(t - T) dT \tag{2.2.1.4}$$

from which we get the moments

$$\langle g_i(t) \rangle = \mu_i \qquad \langle \Delta g_i(t) \Delta g_i(t') \rangle = \frac{\sigma_i^2}{2} e^{-\frac{|t-t'|}{\tau_i}} \tag{2.2.1.5}$$

### 2.2.2 Membrane Potential

We can now work on reconstructing the membrane potential equation (2.1.0.1), using the recently obtained conductances. Substituting the conductances and rearranging the terms we get

$$\frac{dV}{dt} = -\frac{(V - \mu)}{\tau} + \sum_i h_i(V)\eta_i(t) \tag{2.2.2.1}$$

where we have defined a new set of variables

$$\tau = \frac{\tau_L}{1 + \sum_i s_i(V)\mu_i} \tag{2.2.2.2}$$

$$\mu = \frac{\tau}{\tau_L}(E_L + \sum_i s_i(V)\mu_i E_i) \tag{2.2.2.3}$$

$$h_i(V) = s_i(V)\frac{\sqrt{\tau_i}}{\tau_L}\sigma_i(E_i - V) \tag{2.2.2.4}$$

The noise terms are now written as

$$\eta_i(t) = \frac{1}{\tau_i} \int_0^t e^{-\frac{T}{\tau_i}} \xi_i(t - T) dT \tag{2.2.2.5}$$

and have the following correlations

$$\langle \eta_i(t)\eta_i(t')\rangle = \frac{1}{2\tau_i} e^{-\frac{|t-t'|}{\tau_i}} \tag{2.2.2.6}$$

What we have now is a Langevin equation with distinct sources of colored noise. The $n$ dimensional stochastic system is now reduced to 1 stochastic differential equation. This, however, has cost us the markovian property of the noise, i.e, the value of the noise at time $t$ depends on its values at previous times $t' < t$. It makes it impossible to obtain an exact Fokker-Planck equation since it adds an additional time integration. We, therefore, need to construct an approximate Fokker-Planck in order to be able to use the Amit and Brunel method. In some cases, it might also be useful to simplify the problem by finding an approximation that allows us to drop the multiplicative noise.

But first, let's notice some differences in the parameters involved between the standard current-based Langevin equation and the one we found (2.2.2.1). The first one is that the effective membrane time constant now depends on the mean individual currents $\mu_i$. This tells us that the filtering properties of the membrane rely on the input strength so that a time-varying current will impose time-varying filtering of the signal. Specifically, stronger currents decrease the cutoff frequency of the low-pass filter property of the membrane potential.

The second difference is that the mean current behaves as a weighted sum of the reversal potentials instead of a simple sum of the individual means. In this case, the mean currents act like the weights. Therefore the current is limited in the interval determined by the maximal end minimal reversal potential.

Finally, we can see that the noise variance depends on the distance of the membrane potential from the corresponding reversal. This means that the noise is modulated by the membrane potential, and since it also contains the effective membrane time constant, it is modulated by the mean current.

### 2.2.3 Effective Time Constant Approximation

As stated earlier, in some cases we can reduce the complexity of the problem by dropping the multiplicative noise with an appropriate approximation. This can be done by applying what is called the effective time constant approximation (RICHARDSON, 2004)(RICHARDSON; GERSTNER, 2005). It consists of the substitution of the membrane potential in the noise term by the equilibrium potential $\mu$, resulting in

$$h_i(V) \to h_i(\mu)$$

This implies that the modulation of noise can be seen as dependent on the distance of the equilibrium potential from its reversal potential, at least at first order. In fact, it can be

argued that the use of this approximation leads, when the terms $h_i(V)$ are linear, to a more consistent treatment of the problem, since the error generated by this approach is of the same order as the error introduced by the diffusion approximation (RICHARDSON; GERSTNER, 2005). Not only that, but in some cases the errors from both of these sources can partially cancel each other, resulting in a better approximation. But the most important fact here is that this approach simplifies considerably the treatment of the resulting Fokker-Planck equation. A direct consequence of this is that it lends to more easily interpretable parameters.

### 2.2.4 Fox Theory

Temporal correlations in the noise of Langevin equations are known to impede the construction of a exact Fokker-Planck equation. So our task is to find an appropriate approximation that leads to an differential equation of the probability distribution of the membrane potential. There are different ways to approximate this equation: the so-called best Fokker-Planck approximation (SANCHO et al., 1982)(LINDENBERG; WEST, 1983), is one method which supposes a differential form for the diffusion term which is exact in the white noise limit. This differential form is solvable in only particular cases making the use of perturbative methods necessary in most uses. The Fox theory (FOX, 1986a)(FOX, 1986b) uses functional calculus to derive an approximation for small correlations. At first order in the time correlation, both the best Fokker-Planck and the Fox theory give the same result, diverging in higher orders (GRIGOLINI et al., 1988). Jung and Hänggi also derived an approximation which relies in an adiabatic elimination procedure (JUNG; HÄNGGI, 1987). This are only some examples of the different ways to approximate the Fokker-Planck. We use here the Fox theory, since it is the one with the most direct application and is the easiest to generalize for multiple noise sources.

In this section, we will take a detour to give a brief explanation of this method and expand the original derivation to multiple decorrelated noise sources. This will be used in the sequence to obtain an appropriate Fokker-Planck so that we can formulate an equation for the probability distribution of $V$. The Fox theory, as stated, is based on a functional calculus approach to the Langevin equations. So, instead of drawing the stochastic variable from a gaussian distribution at each point in time, we draw the entire trajectory of the stochastic variable from a functional Gaussian distribution (figure 6). The original derivation of the Fox theory is valid for a single source of the noise. Since in our case we have different sources of noise with different correlation times, we need to expand the method. This exposition is, therefore, heavily based on the original papers by Fox (FOX, 1986a)(FOX, 1986b).

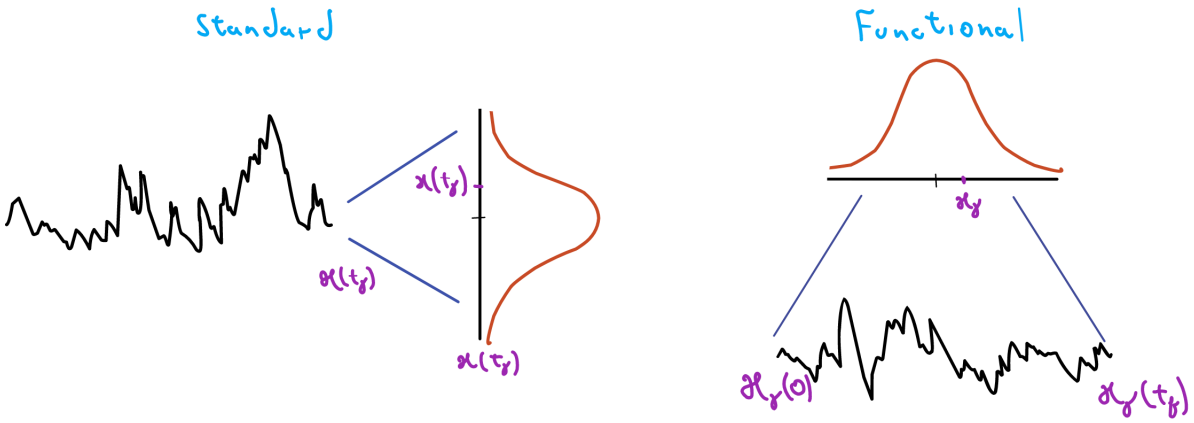


Figure 6 – Schematics of the difference between the standard approach to the Fokker-Planck equation construction and the functional one.

Lets first define our generic stochastic differential equation in the variable $x$,

$$\frac{dx}{dt} = W(x) + h_1(x)\eta_1(t) + h_2(x)\eta_2(t)\,, \tag{2.2.4.1}$$

where $W(x)$ is our drift term, $h_1(x)$ and $h_2(x)$ the multiplicative term, and $\eta_1$ and $\eta_2$ are the colored noises in the system. For simplicity, we use two noise sources in this derivation, but the generalization for $n$ sources is trivial. As stated, we treat the noise in a functional form, drawing the entire trajectory from an appropriate Gaussian distribution. These distributions are given by

$$\mathcal{P}_i[\eta_i] = N_i \exp\left(-\frac{1}{2}\int ds \int ds'\eta_i(s)\eta_i(s')K_i(s-s')\right)\,, \tag{2.2.4.2}$$

where $i \in \{1,2\}$ is the noise index. The normalization constant $N_i$ is calculated by integrating over all paths that $\eta_i$ can take:

$$N_i^{-1} = \int \mathcal{D}\eta_i \exp\left(-\frac{1}{2}\int ds \int ds'\eta_i(s)\eta_i(s')K_i(s-s')\right)\,. \tag{2.2.4.3}$$

We also have the kernel $K_i$ which correspond to the inverse of the correlation function of the noise. Let the noise correlation be described by

$$\langle \eta_i(t)\eta_i(t')\rangle = C_i(t-t')\,. \tag{2.2.4.4}$$

This implies that the kernel $K_i$ has the form

$$\int K_i(t-t')C_i(t'-s)dt' = \delta(t-s)\,. \tag{2.2.4.5}$$

If the noise is white, the correlation is a delta function $C_i(t-s) = A\delta(t-s)$ and therefore the kernel is also a delta function $K_i = A^{-1}\delta(t-t')$. For a colored noise, the kernel will

depend on the functional form of $C_i$. We assume here that the noises are independent from each other, which means that

$$\mathcal{P}[\eta] \equiv \mathcal{P}[\eta_1, \eta_2] = \mathcal{P}_1[\eta_1]\mathcal{P}_2[\eta_2]\,. \tag{2.2.4.6}$$

We start by writing the probability of a specific path $y$

$$P(y,t) = \int \mathcal{D}\eta\mathcal{P}[\eta]\delta(y - x(t))\,. \tag{2.2.4.7}$$

The symbol $\int \mathcal{D}\eta$ is defined as the path integral taken over both noise variables, that is, $\int \mathcal{D}\eta = \int \mathcal{D}\eta_1 \int \mathcal{D}\eta_2$. Deriving with respect to time gives

$$\frac{\partial P}{\partial t} = -\int \mathcal{D}\eta\mathcal{P}[\eta]\frac{\partial}{\partial y}\delta(y - x(t))\frac{dx}{dt}\,. \tag{2.2.4.8}$$

We can now substitute (2.2.4.1) to get

$$\frac{\partial P}{\partial t} = -\frac{\partial}{\partial y}[W(y)P] - \frac{\partial}{\partial y}h_1(y)\int \mathcal{D}\eta\mathcal{P}[\eta]\eta_1(t)\delta(y-x(t)) - \frac{\partial}{\partial y}h_2(y)\int \mathcal{D}\eta\mathcal{P}[\eta]\eta_2(t)\delta(y-x(t))\,. \tag{2.2.4.9}$$

From now on, lets focus only on the first integral, since the procedure is similar for the second. To be able to get the correspondent diffusion term, we need to resolve the expression $\mathcal{P}[\eta]\eta_1(t)$. This can be done by writing

$$\mathcal{P}[\eta]\eta_1(t) = \mathcal{P}[\eta]\int ds\delta(t-s)\eta_1(s) = \mathcal{P}[\eta]\int ds\int ds' C_1(t-s')K_1(s'-s)\eta_1(s) = \\ = -\int ds' C_1(t-s')\frac{\delta\mathcal{P}[\eta]}{\delta\eta_1(s')}\,, \tag{2.2.4.10}$$

where we used the delta identity (2.2.4.5) in the second step and the functional derivative of the distribution

$$\frac{\delta\mathcal{P}[\eta]}{\delta\eta_1(s')} = -\mathcal{P}[\eta]\int ds K_1(t-s)\eta_1(s) \tag{2.2.4.11}$$

in the third step. Substituting in the integral of (2.2.4.9) and using functional integration by parts, it becomes

$$\int \mathcal{D}\eta P[\eta]\eta_1(t)\delta(y-x(t)) = -\int ds' C_1(t-s')\int \mathcal{D}\eta P[\eta]\frac{\partial}{\partial y}\delta(y-x(t))\frac{\delta x(t)}{\delta\eta_1(s')}\,. \tag{2.2.4.12}$$

The problem now is the functional derivative on $x(t)$. For this, we take the respective functional derivative of (2.2.4.1)

$$\frac{d}{dt}\frac{\delta x(t)}{\delta\eta_1(s')} = W'(x)\frac{\delta x(t)}{\delta\eta_1(s')} + h_1(x)\delta(t-s') + h_1'(x)\frac{\delta x(t)}{\delta\eta_1(s')}\eta_1(t) + h_2'(x)\frac{\delta x(t)}{\delta\eta_1(s')}\eta_2(t) \tag{2.2.4.13}$$

This differential equation in $\frac{\delta x(t)}{\delta\eta_1(s')}$ can be solved to yield

$$\frac{\delta x(t)}{\delta\eta_1(s')} = \Theta(t-s')h_1(x(s'))\exp\left(\int_{s'}^{t} ds[W'(x(s)) + h_1'(x(s))\eta_1(s) + h_2'(x(s))\eta_2(s)]\right) \tag{2.2.4.14}$$

We can now substitute this expression and the correspondent one for the second integral in (2.2.4.12) and get the full exact equation on the distribution

$$\frac{\partial P}{\partial t} = -\frac{\partial}{\partial y}[W(y)P] + \frac{\partial}{\partial y}h_1(y)\frac{\partial}{\partial y}\int_0^t ds' C_1(t-s')\times$$
$$\times\int \mathcal{D}\eta P[\eta]\delta(y-x(t))\exp\left(\int_{s'}^t ds[W'(x(s)) + h_1'(x(s))\eta_1(s) + h_2'(x(s))\eta_2(s)]\right)h_1(x(s'))+\dots\,, \tag{2.2.4.15}$$

where we hid the second integration term for the sake of clarity. We can see here the non-markovian property of the process. The equation of the probability distribution depends on previous times by the correlation kernel $C_1$ and $C_2$. It can also be seen that a white noise correlation $C_i(t-s') = \delta(t-s')$ will result in the well known Fokker-Planck equation.

We will get rid of the time integration in the exponential by taylor expanding the integral. But first, lets evolve $h_1(s')$ until $t$.

$$\frac{d}{dt}h_1(x(t)) = h_1'(x(t))\dot{x}(t) = \frac{h_1'(x(t))}{h_1(x(t))}[W(x(t)) + h_1(x(t))\eta_1(t) + h_2(x(t))\eta_2(t)]h_1(x(t))\,. \tag{2.2.4.16}$$

The formal solution for $h(x(s'))$ is then

$$h_1(x(s')) = \exp\left(\int_t^{s'} ds\frac{h_1'(x(t))}{h_1(x(t))}[W(x(t)) + h_1(x(t))\eta_1(t) + h_2(x(t))\eta_2(t)]\right)h_1(x(t))\,. \tag{2.2.4.17}$$

We can now introduce the form of interest of our correlation function, that is, an exponentially decaying function

$$\langle\eta_i(t)\eta_i(s)\rangle = C_i(t-s) = \frac{D_i}{\tau_i}\exp\left(-\frac{|t-s|}{\tau_i}\right). \tag{2.2.4.18}$$

Proceeding to substitute (2.2.4.17) and (2.2.4.18) in (2.2.4.15) results in

$$\frac{\partial P}{\partial t} = -\frac{\partial}{\partial y}[W(y)P] + \frac{\partial}{\partial y}h(y)\frac{\partial}{\partial y}\int_0^t ds'\frac{D_1}{\tau_1}\exp\left(-\frac{|t-s|}{\tau_1}\right)\int \mathcal{D}\eta\mathcal{P}[\eta]\delta(y-x(t))$$
$$\times\exp\left(\int_{s'}^t ds\left[W'(x(s)) + \frac{h_1'(x(s))}{h_1(x(s))}W(x(s)) + \left(h_2'(x(s)) - \frac{h_1'(x(s))}{h_1(x(s))}h_2(x(s))\right)\eta_2(s)\right]\right)h_1(x(t))+\dots\,. \tag{2.2.4.19}$$

Our first approximation here is to use the average of the noise instead of the noise in the exponential. This means that, since the average is zero, the cross dependence of the $\eta_2$ term in the first path integral (and similarly, the dependence of $\eta_1$ in the second) is dropped. This procedure can be shown to be self consistent in the sense that it correctly reduces to the adequate additive noise case. You can note that both noise terms in (2.2.4.13) are zero in the additive case and therefore a cross-term don't appear. The same procedure was used in the first derivation of the Fox theory (FOX, 1986a).

We can now change the integration variable $s'$ to $\theta_1 = (t - s')/\tau_1$ (similarly for the second integral term) and expand the integral in the exponential for $\tau_1 \to 0$, resulting in

$$D_1 \int_0^{t/\tau_1} d\theta_1 e^{-\theta_1} \int \mathcal{D}\eta \mathcal{P}[\eta] \delta(y - x(t)) \exp\left[\int_{t-\tau_1\theta_1}^{t} ds \left(W'(x(s)) - \frac{h_1'(x(s))}{h_1(x(s))} W(x(s))\right)\right] h_1(x(t)) \underset{\tau_1 \to 0}{\approx}$$
$$\underset{\tau_1 \to 0}{\approx} D_1 \int_0^{\infty} d\theta_1 e^{-\theta_1} \int \mathcal{D}\eta \mathcal{P}[\eta] \delta(y - x(t)) \exp\left[\tau_1\theta_1 \left(W'(x(s)) - \frac{h_1'(x(s))}{h_1(x(s))} W(x(s))\right)\right] h_1(x(t)) =$$
$$= \frac{D_1 h_1(y)}{1 - \tau_1 \left(W'(y) - \frac{h_1'(y)}{h_1(y)} W(y)\right)} P(y,t)\,. \quad (2.2.4.20)$$

Therefore we arrive at our effective Fokker-Planck equation for two sources of colored multiplicative noise

$$\frac{\partial P(y,t)}{\partial t} = -\frac{\partial}{\partial y}\left[W(y)P(y,t)\right] + D_1 \frac{\partial}{\partial y}\left\{h_1(y)\frac{\partial}{\partial y}\left[\frac{h_1(y)}{1 - \tau_1\left(W'(y) - \frac{h_1'(y)}{h_1(y)}W(y)\right)} P(y,t)\right]\right\} +$$
$$+ D_2 \frac{\partial}{\partial y}\left\{h_2(y)\frac{\partial}{\partial y}\left[\frac{h_2(y)}{1 - \tau_2\left(W'(y) - \frac{h_2'(y)}{h_2(y)}W(y)\right)} P(y,t)\right]\right\}. \quad (2.2.4.21)$$

The Fokker-Planck approximation presented here does have some interesting properties that are relevant to this work. First of all, it is important to note that the approach followed in this method is not perturbative. In fact, under a certain condition, the convergence of the approximation for $\tau_i \to 0$ is uniform, that is, it converges to the white noise case for all values of $y$ in the domain of interest (FOX, 1986b). The uniformity condition is

$$1 - \tau_i \left(W'(y) - \frac{h_i'(y)}{h_i(y)} W(y)\right) > 0\,. \quad (2.2.4.22)$$

This condition gives us a form of metric of $\tau_i$ for which we can expect the approximation to behave reasonably well.

Another property was found by Jung and Hänggi (JUNG; HÄNGGI, 1987). Their adiabatic method resulted in an approximation that is valid for small and large values $\tau_i$. They noted, however, that the stationary solution of the Fox theory agrees with their stationary solution. Therefore, even though the resulting effective Fokker-Planck obtained by the Fox theory was derived for small $\tau_i$ values, the stationary solution is valid also for large $\tau_i$ (given that condition (2.2.4.22) is obeyed). The validity for both limits suggests that the Fox theory is a good interpolation between both stationary results. A small derivation of the validity of the stationary solution of the Fox theory for $\tau_i \to \infty$ can also be found in (GRIGOLINI et al., 1988).

### 2.2.5 Transfer Function

After this detour, we have in our hands all the tools needed to solve the problem. The Langevin equation using the effective time constant approximation can be written as

$$\frac{dV}{dt} = -\frac{(V-\mu)}{\tau} + \sum_i h_i(\mu)\eta_i(t)\,. \tag{2.2.5.1}$$

A straightforward application of (2.2.4.21) results in the corresponding effective Fokker-Planck equation of interest

$$\frac{\partial P(V,t)}{\partial t} = \frac{\partial}{\partial V}\left[\frac{(V-\mu)}{\tau}P(V,t)\right] + \frac{1}{2\tau}\left[\sum_i \frac{\tau^2}{\tau+\tau_i}h_i^2\right]\frac{\partial^2 P(V,t)}{\partial V^2}\,, \tag{2.2.5.2}$$

where we have simplified the notation by calling $h_i(\mu) = h_i$.

This Fokker-Planck has the same form as the one derived for the current-based integrate-and-fire model (CuBa-IFM) (1.3.0.5). The comparison establishes a relationship between the noise variance of the CuBa-IFM and the diffusion coefficient of our CoBa-IFM result. We can state this relationship as follows

$$\sigma_V^2 = \sum_i \sigma_{V_i}^2 = \sum_i \frac{\tau^2}{\tau+\tau_i}h_i^2\,, \tag{2.2.5.3}$$

where the independence of the terms in the sum suggests the separation of the full variance in two independent components. There is, then, a simple interpretation of the parameters of the effective Fokker-Planck equation. The first-order term (the drift term) corresponds to the deterministic drive of the membrane potential, as is in the CuBa-IFM. The second-order term (the diffusion term) can be seen as the sum of the variance of the noise sources, where the noise sources are treated as white. The combination of both approximations (effective time-constant and the Fox theory), therefore, produces the same behavior as the following Langevin system:

$$\frac{dV}{dt} = -\frac{(V-\mu)}{\tau} + \sigma_V\xi(t) \tag{2.2.5.4}$$

Since the Fokker-Planck (2.2.5.2) has the same form as (1.3.0.5), we can take the same solution (1.3.0.9) and apply it with our set of parameters

$$\frac{1}{\nu} = \tau_r + \tau\sqrt{\pi}\int_{\frac{V_r-\mu}{\sigma_V}}^{\frac{\theta-\mu}{\sigma_V}} e^{x^2}(1+\mathrm{erf}(x))dx \tag{2.2.5.5}$$

where $\sigma_V$ is given by (2.2.5.3), $\mu$ by (2.2.2.3), and $\tau$ by (2.2.2.2). We can also get the stationary probability distribution

$$P_s(V) = \frac{2\nu\tau}{\sigma_V}\exp\left(-\frac{(V-\mu)^2}{\sigma_V^2}\right)\int_{\frac{V-\mu}{\sigma_V}}^{\frac{\theta-\mu}{\sigma_V}} \Theta\left(x - \frac{V_r-\mu}{\sigma_V}\right)e^{x^2}dx \tag{2.2.5.6}$$

### 2.2.6 Multiplicative Noise

In some cases, the effective time constant approximation is not appropriate or cannot be used. Specifically, when the multiplicative noise terms are nonlinear, we need to carry the full-terms to the Fokker-Planck equation. Let's tackle the full-multiplicative noise problem, then. We begin with the generic Langevin equation, written as

$$\frac{dV}{dt} = W(V) + \sum_i h_i(V)\eta_i(t)\,. \tag{2.2.6.1}$$

where $W(V) = -(V-\mu)/\tau$. We note that since $\mu$ and $\tau$ depend on $s_i$, which can be a function of $V$, both can also be functions of $V$. Applying the result of the Fox theory lead us to the following effective Fokker-Planck equation

$$\frac{\partial P}{\partial t} = -\frac{\partial}{\partial V}\left[W(V)P\right] + \sum_i \frac{1}{2}\frac{\partial}{\partial V}\left\{h_i(V)\frac{\partial}{\partial V}\left[\frac{h_i(V)}{1-\tau_i(W'(V)-\frac{h_i'(V)}{h_i(V)}W(V)}P\right]\right\}. \tag{2.2.6.2}$$

We can simplify the notation by introducing new variables

$$S_i(V) = \frac{1}{2}\left[\frac{h_i(V)}{1-\tau_i(W'(V)-\frac{h_i'(V)}{h_i(V)}W(V)}\right] \tag{2.2.6.3}$$

The differential equation has now the form

$$\frac{\partial P}{\partial t} = -\frac{\partial}{\partial V}\left[W(V)P - \sum_i h_i(V)\frac{\partial}{\partial V}(S_i(V)P)\right] \tag{2.2.6.4}$$

This can be written in the form of a continuity equation

$$\frac{\partial P}{\partial t} = -\frac{\partial J}{\partial V}\,, \tag{2.2.6.5}$$

where

$$J = W(V)P - \sum_i h_i(V)\frac{\partial}{\partial V}(S_i(V)P)\,. \tag{2.2.6.6}$$

In the steady-state, $\frac{\partial P_s}{\partial t} = 0$. This means that $J$ is constant in the whole domain, except in the discontinuity points $V_r$ and $\theta$. In the threshold $\theta$, we also have an absorbing boundary condition. The absorbed probability current corresponds to the firing rate $\nu$ and is reintroduced in the reset potential $V_r$ after the refractory period $\tau_r$. We can therefore write the current as

$$J = \nu\Theta(V-V_r) = W(V)P_s - \sum_i h_i(V)\frac{\partial}{\partial V}(S_i(V)P_s)\,, \tag{2.2.6.7}$$

where $\Theta$ is the Heaviside function. We now have a first-order linear differential equation on $P_s$. Proceeding to solve it via integrating factor, lets first rewrite it in a more explicit form

$$\frac{\partial P_s}{\partial V} + \frac{\left[\sum_i h_i(V)\frac{dS_i}{dV} - W(V)\right]}{\sum_i h_i(V)S_i(V)}P_s = -\frac{\nu\Theta(V-V_r)}{\sum_i h_i(V)S_i(V)}\,. \tag{2.2.6.8}$$

Defining new variables

$$\chi(V) = \sum_i h_i(V) S_i(V)\,, \tag{2.2.6.9}$$

$$B(V) = \frac{\sum_i h_i(V)\frac{dS_i}{dV} - W(V)}{\chi(V)}\,. \tag{2.2.6.10}$$

We can now multiply by the integrating factor $e^{\int B(V)dV} = e^{F(V)}$ and integrate from $V$ to $\theta$ to get

$$P_s(V) = \nu \int_V^\theta e^{F(x)-F(V)} \frac{\Theta(x - V_r)}{\chi(x)} dx\,. \tag{2.2.6.11}$$

Using the normalization condition

$$\int_{-\infty}^{\theta} P_s(V)dV + \nu\tau_r = 1\,, \tag{2.2.6.12}$$

we can substitute the probability expression to get

$$\frac{1}{\nu} = \tau_r + \int_{-\infty}^{\theta}\int_V^\theta \frac{\Theta(x - V_r)}{\chi(x)} e^{F(x)-F(V)} dxdV\,. \tag{2.2.6.13}$$

We can finally change the integration order to arrive in the expression for $\nu$

$$\frac{1}{\nu} = \tau_r + \int_{V_r}^{\theta}\int_{-\infty}^{x} \frac{e^{F(x)-F(V)}}{\chi(x)} dVdx \tag{2.2.6.14}$$

The lower limit of the first interval can be limited by the lowest of the reversal potentials, since the dynamics of the membrane potential cannot be lower than this value. But in a general sense, the infinity can be written in place as we did.

This formal solution, unfortunately, is not straightforward to use since a closed form for the integrating factor is generally not obtainable. Also, it is necessary to carefully evaluate the existence of poles in the differential equation, which we did not do here. Therefore, to get numerical results for the firing rate transfer function we made use of a numerical procedure.

## 2.3 Numerical Approach

We can numerically integrate the differential equation to get the results for $P$ and $\nu$. The most direct way of doing this would be to use the Euler method, but since we have a formal solution, we can use it to make a better integration procedure with better convergence properties. This method was developed by [Richardson:2007], and we will describe it in the following.

First lets rewrite our differential equation in $P_s$

$$\frac{\partial P_s}{\partial V} + B(V)P_s = -\frac{\nu\Theta(V - V_r)}{\chi(V)}\,. \tag{2.3.0.1}$$

To get rid off the firing rate term, we can define the rescaled variable $p_0$ as $P_s = p_0\nu$. Therefore, our equation becomes independent of $\nu$

$$-\frac{\partial p_0}{\partial V} = B(V)p_0 + H(V)\,, \tag{2.3.0.2}$$

where we defined $H(V) = \frac{\Theta(V-V_r)}{\chi(V)}$. We then divide the integration interval (in our case $(E_I, \theta)$) in steps of size $\Delta$, giving us the points $V^{(k)} = E_I + \Delta k$. This implies that $V^{(0)} = E_I$ and $V^{(N)} = \theta$. In this division, is also convenient to have a $k$ such that $V^{(k)} = V_r$, so that the discontinuity lies in one of the points. Integrating in one step, we get

$$p_0^{(k-1)} = p_0^{(k)} e^{\int_{V^{(k-1)}}^{V^{(k)}} B(V)dV} + \int_{V^{(k-1)}}^{V^{(k)}} H(V) e^{\int_{V^{(k-1)}}^{V} B(U)dU} dV\,. \tag{2.3.0.3}$$

Expanding $B$ and $H$ around $V^{(k)}$ to zeroth order in $\Delta$, we get

$$p_0^{(k-1)} \approx p_0^{(k)} e^{\Delta B^{(k)}} + \Delta H^{(k)} \left( \frac{e^{\Delta B^{(k)}} - 1}{\Delta B^{(k)}} \right)\,, \tag{2.3.0.4}$$

where $B^{(k)} = B(V^{(k)})$ and $H^{(k)} = H(V^{(k)})$. Since we know that $p_0(\theta) = 0$, we can reverse integrate $p_0$ using this recursion relation. From the definition of $p_0$ and the normalization condition (2.2.6.12) we get

$$\nu = \frac{1}{\tau_r + \sum_{k=0}^{N} \Delta p_0^{(k)}}\,. \tag{2.3.0.5}$$

Substituting this expression in the definition $P_s = p_0\nu$ results in the stationary probability distribution

$$P_s = \frac{p_0}{\tau_r + \sum_{k=0}^{N} \Delta p_0^{(k)}}\,. \tag{2.3.0.6}$$

# 3 Results

## 3.1 Conductance-Based Integrate-and-Fire Neuron

We will first apply our model to a simple conductance-based integrate-and-fire neuron with two input channels: an excitatory $g_E(t)$, and an inhibitory $g_I(t)$ channel. So the equations describing our system are

$$\tau_L \frac{dV}{dt} = -(V - E_L) - g_E(t)(V - E_E) - g_I(t)(V - E_I)\,, \tag{3.1.0.1}$$

$$\tau_E \frac{dg_E}{dt} = -g_E + \sum_{j,k} w_E \delta(t - t_j^k)\,, \tag{3.1.0.2}$$

$$\tau_I \frac{dg_I}{dt} = -g_I + \sum_{j,k} w_I \delta(t - t_j^k)\,. \tag{3.1.0.3}$$

The neuron also receives input from $K_E$ excitatory input neurons and $K_I$ inhibitory. Both populations fire at a rate $\nu_i$. The neuron fire if the potential reaches the threshold $\theta$ and then the potential is reset to $V_r$ for a period $\tau_R$. To be able to simulate this system, specific values are needed to be attributed to the parameters. The values are taken to be physiologically plausible and are in the range of typically used values in simulated works, for example, in (ZENKE; AGNES; GERSTNER, 2014). The specific values are listed in table 1.

| **Variable** | **Value** |
|---|---|
| $E_L$ | -60mV |
| $E_E$ | 0mV |
| $E_I$ | -80mV |
| $w_E$ | {0.1, 0.5} |
| $w_I$ | {0.1, 0.4, 1.0, 10.0} |
| $\tau_L$ | 20ms |
| $\tau_E$ | variable |
| $\tau_I$ | 10ms |
| $\tau_R$ | 2ms |
| $K_E$ | 400 |
| $K_I$ | 100 |
| $\theta$ | -50mV |
| $V_r$ | -60mV |
| $\nu_i$ | {5, 20, 50}Hz |

Table 1 – Table containing the set of parameters used for the simple Conductance-Based Integrate-and-Fire model.

As a way to demonstrate the validity of the diffusion approximation, for the range of values used here, we plotted the mean, the standard deviation, and the skewness of the analytical conductance and the simulated one (figure 7). As expected by the construction, the expressions for the mean and the standard deviation are good representation of the values simulated even when the synaptic weight $w_E$ is large. In contrast, we can see deviations in the skewness for small values of $\tau_E$. This is somewhat expected since the values of $g(t)$ can't be negative and the diffusion approximation don't take this into consideration. Therefore, for small $\tau_E$, we have small $\mu_E$ and the Gaussian form of the approximation fails to account the asymmetric shape of the distribution with a hard boundary at $g = 0$. Therefore, as stated by (RICHARDSON; GERSTNER, 2005), the diffusion approximation introduce errors at the third order moment of the distribution.

Proceeding, the form of the Langevin equation for the Conductance-Based Integrate-and-Fire is

$$\frac{dV}{dt} = -\frac{(V-\mu)}{\tau} + h_E(V)\eta_E(t) + h_I(V)\eta_I(t)\,, \tag{3.1.0.4}$$

where

$$\tau = \frac{\tau_L}{1+\mu_E+\mu_I}\,, \tag{3.1.0.5}$$

$$\mu = \frac{\tau}{\tau_L}(E_L + \mu_E E_E + \mu_I E_I)\,, \tag{3.1.0.6}$$

$$h_{E,I}(V) = \frac{\sqrt{\tau_{E,I}}}{\tau_L}\sigma_{E,I}(E_{E,I} - V)\,. \tag{3.1.0.7}$$

We can now use the effective time-constant approximation or deal with the full multiplicative problem. Lets first apply the approximation and see what it results.

### 3.1.1 Additive Noise

With the effective time-constant approximation, the Langevin simplify to

$$\frac{dV}{dt} = -\frac{(V-\mu)}{\tau} + h_E\eta_E(t) + h_I\eta_I(t)\,, \tag{3.1.1.1}$$

where the constant coefficients are $h_E = h_E(\mu)$ and $h_I = h_I(\mu)$. Application of the Fox theory results in the transfer function (2.2.5.5) and the probability distribution (2.2.4.15) with the expression for $\sigma_V$ given by

$$\sigma_V^2 = \frac{\tau^2}{\tau+\tau_E}h_E^2 + \frac{\tau^2}{\tau+\tau_I}h_I^2\,. \tag{3.1.1.2}$$

A comparison of the analytical results (numerically integrated as explained in section 2.3) with the simulations can be seen in figure 8. Good agreement is present for all variables calculated with this set of parameters. Changing the input rate $\nu_i$ has little effect on the stationary potential $\mu$ but changes the noise variance $\sigma_V^2$ of the neuron without threshold.

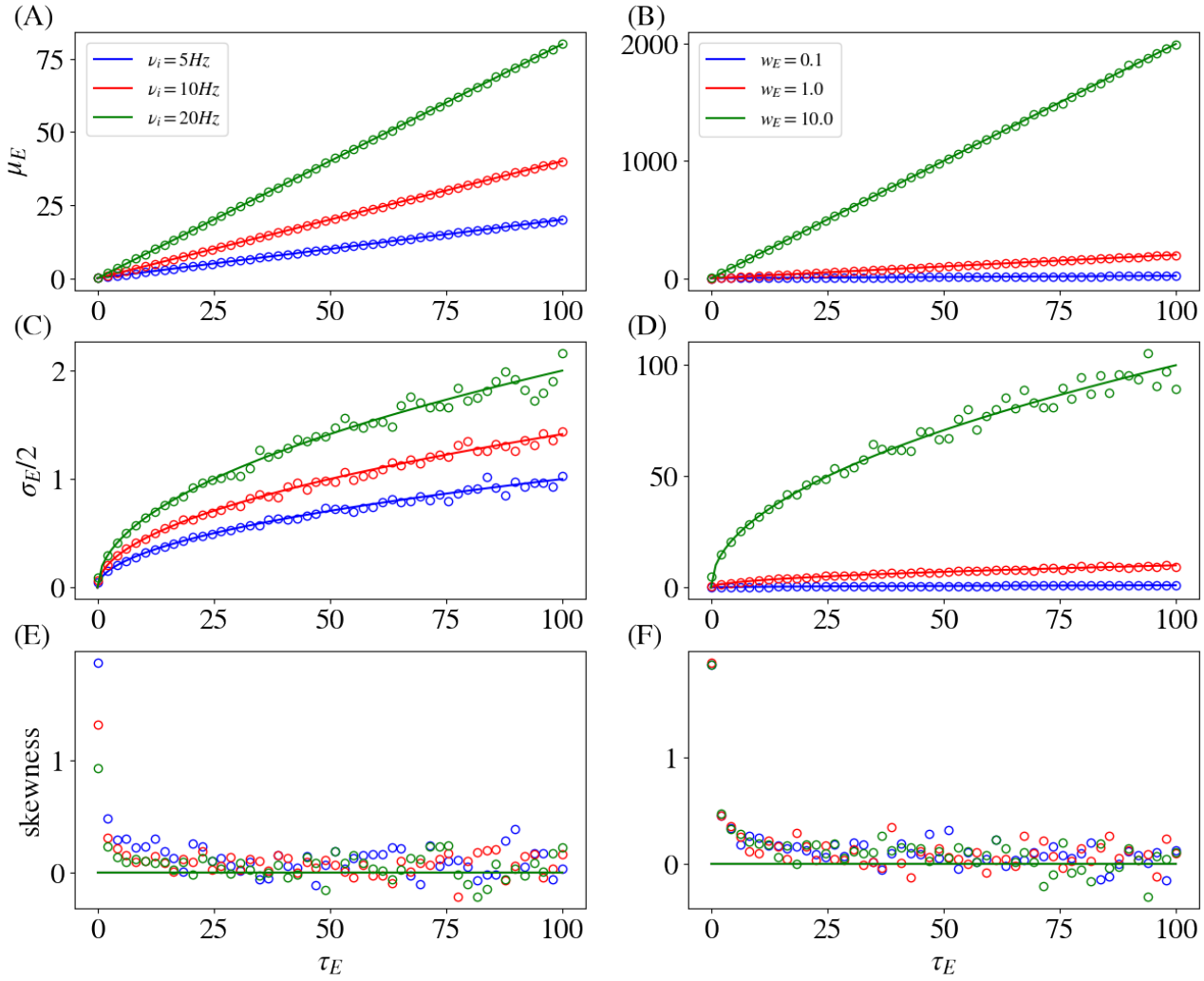


Figure 7 – Comparison of the analytical expressions obtained for the statistics of $g_E$ using the diffusion approximation (lines) with simulations (circles). We can see that the analytical expressions are good descriptions of the simulations for all the range of parameters tested for the first and second moments. The skewness, however, exhibits a deviation from the Gaussian approximation for small $\tau_E$. Parameters for first column, $w_E = 0.1$, $w_I = 0.4$; second column, $w_I = 0.8$, $\nu_i = 5Hz$

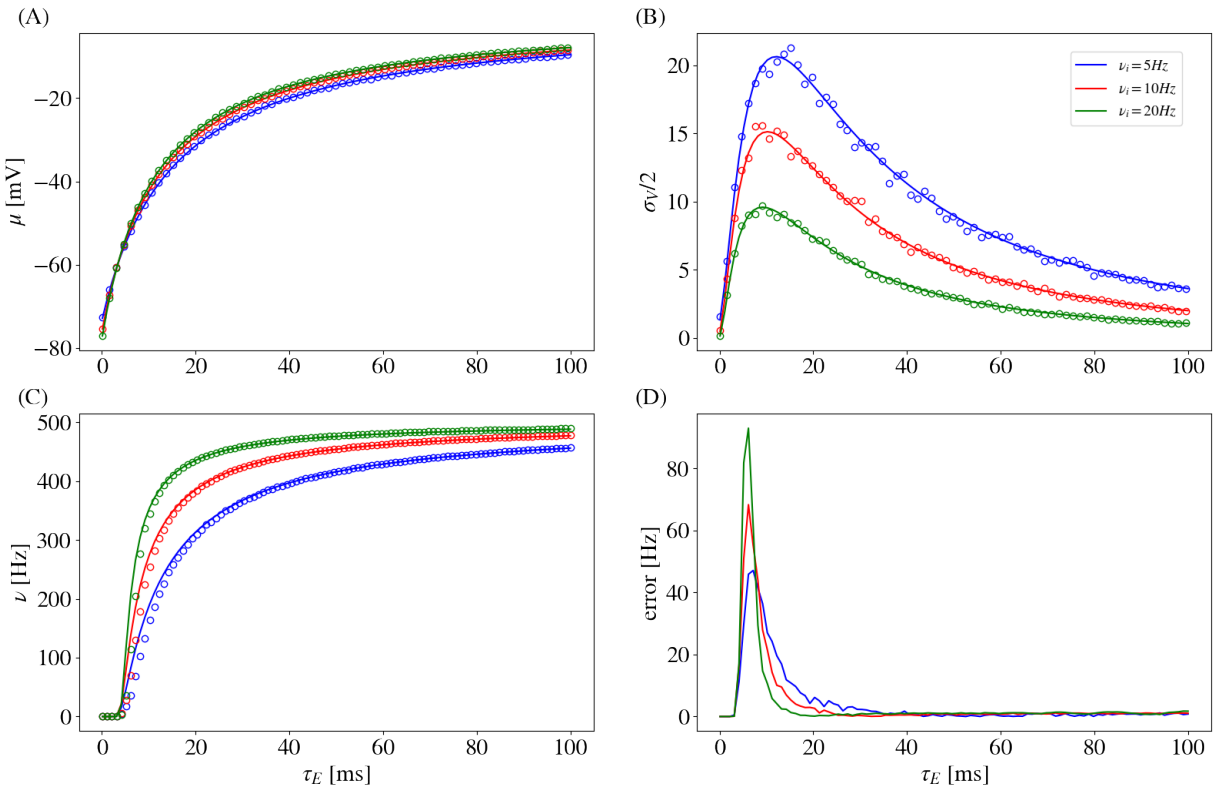


Figure 8 – Comparison of the analytical model with simulations for the simple conductance-based integrate-and-fire neuron using the effective time-constant approximation. Three different values of input firing rate $\nu_i$ as a function of the excitatory time constant. (A) Mean potential for a thresholdless model. (B) Standard deviation of the membrane potential for the same thresholdless model. (C) Firing rate and (D) absolute error between the the analytical firing rate and simulations. Absolute error was calculated as the absolute value between both measures. Relevant parameters are $w_E = 0.1$, $w_I = 0.4$.

So the variation in the firing rate is mostly given by the changes in the variance in this case. A higher noise variance makes the transition from silent to firing smoother. This behavior can be intuited by picturing a moving Gaussian: changing the time constant $\tau_E$ has as one of its effects moving the distribution towards the threshold. Since the firing rate is equal to the probability current at the threshold, and this current is proportional to the derivative of the distribution at the same point (equation (2.2.6.7), noting that $P_s(\theta) = 0$), this derivative has a smoother transition when the variance is larger. Therefore, the firing rate also increases more smoothly. From figure 8C and 8D we can also note that the error concentrate in the region of transition.

Lets now evaluate the model for different inhibition levels by increasing the inhibitory synaptic weight $w_I$ (figure 9). We use three values of inhibitory synaptic weight: $w_I = 0.1$, $w_I = 1.0$, and $w_I = 10.0$ with a constant excitatory weight $w_E = 0.5$. It is possible to see again a good agreement for the mean and variance. For the firing rate, however, the curve for $w_I = 10.0$ has a sharper transition than expected. We can also

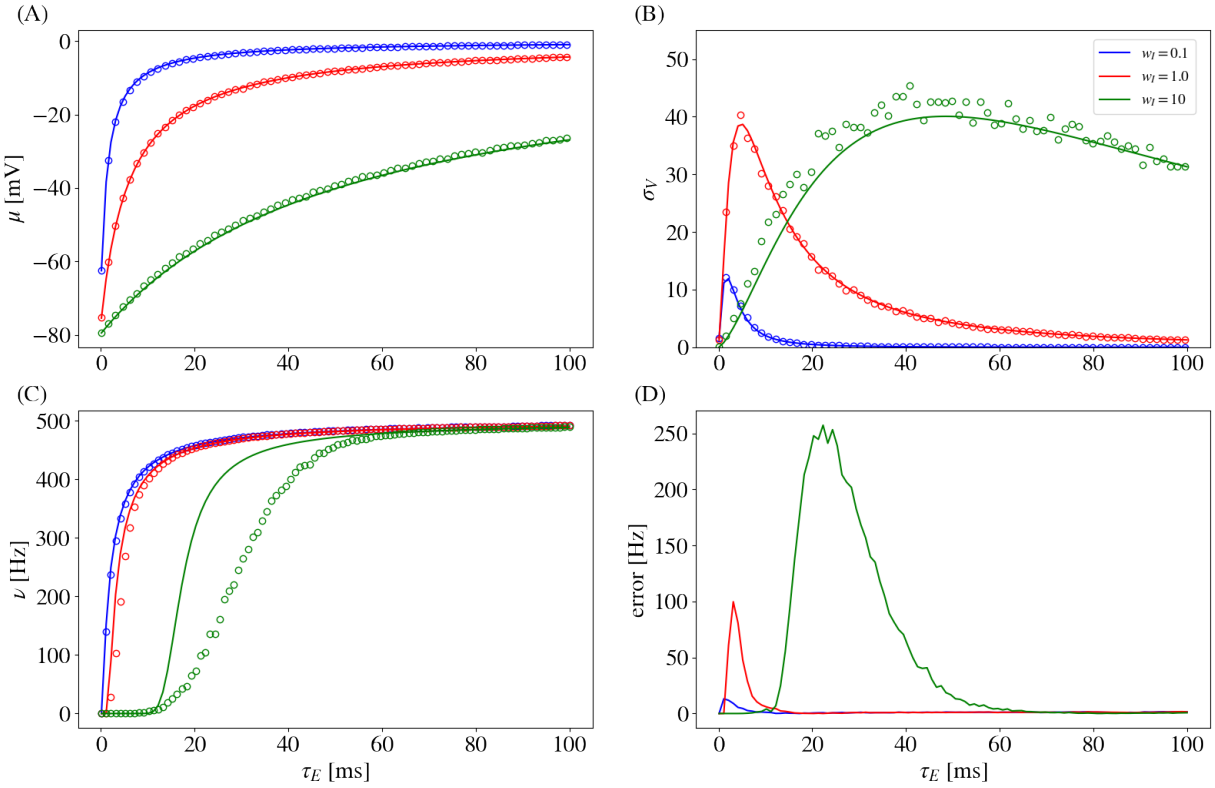


Figure 9 – Comparison of the analytical model with simulations for the simple conductance-based integrate-and-fire neuron using the effective time-constant approximation. Three different values of inhibitory synaptic weight $w_I$ as a function of the excitatory time constant. (A) Mean potential for a thresholdless model. (B) Standard deviation of the membrane potential for the same thresholdless model. (C) Firing rate and (D) absolute error between the the analytical firing rate and simulations. Relevant parameters are $w_E = 0.5$, $\nu_i = 5Hz$.

see that the error is larger in the region where $\mu$ is between $E_L$ and $\theta$, that is, in the sub-threshold regime. In this region spikes are driven by fluctuations in the membrane potential. The sharpness of the transition compared to the data suggests that in this, for those parameters values, the model underestimates the fluctuations. We can examine what differences the introduction of the full multiplicative noise produce compared to the simplified one.

### 3.1.2 Multiplicative Noise

The full-multiplicative noise results in a Fokker-Planck equation with the form

$$\frac{\partial P}{\partial t} = -\frac{\partial}{\partial V}\left[W(V)P\right] + \frac{\partial}{\partial V}h_E(V)\frac{\partial}{\partial V}\left(S_E(V)P\right) + \frac{\partial}{\partial V}h_I(V)\frac{\partial}{\partial V}\left(S_I(V)P\right)\,, \quad (3.1.2.1)$$

where the functions $S_E(V)$ and $S_I(V)$ are given by the generic expression in (2.2.6.3). The stationary differential equation that will be solved numerically is then

$$\frac{\partial P_s}{\partial V} + B(V)P_s = -\nu H(V)\,, \quad (3.1.2.2)$$

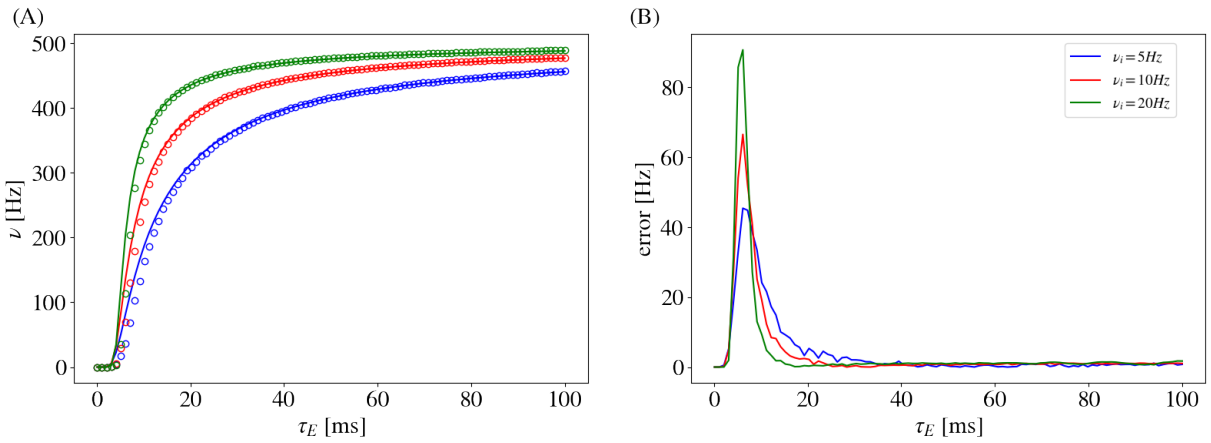


Figure 10 – Comparison of the analytical model with simulations for the simple conductance-based integrate-and-fire neuron using the full-multiplicative model. Three values of input firing rate were tested. (A) Firing rate and (B) absolute error between the the analytical firing rate and simulations. Relevant parameters are $w_E = 0.1$, $w_I = 0.4$.

with

$$B(V) = \frac{h_E(V)S'_E(V) + h_I(V)S'_I(V) - W(V)}{\chi(V)}\,, \tag{3.1.2.3}$$

$$H(V) = \frac{\Theta(V - V_r)}{\chi(V)}\,, \tag{3.1.2.4}$$

$$\chi(V) = h_E(V)S_E(V) + h_I(V)S_I(V)\,. \tag{3.1.2.5}$$

With this in our hands, we solved again the stationary Fokker-Planck numerically for the same set of parameters as in the last subsection. For the different input firing rates, no appreciable differences can be seen between the additive model and the multiplicative one (figure 10). However, a considerable difference appears when we look at the higher value of inhibitory weight $w_I = 10.0$ (figure 11). At a first glance, the treatment of the full multiplicative noise appears to result in a worst solution to the problem, since the error increases a little in the transition region. But a closer inspection of the form of the curves reveals a better qualitative behavior since both the analytical curve and the simulation data have the same shape. In fact, it seems that a translation of the curve in the $\tau_E$ axis would make it fit the data almost perfectly. Therefore, an improvement can probably be obtained by comparing the error for different parameters and fitting an appropriate translation. We suspect that the multiplicative treatment improves the variance estimation but underestimates the mean.

To finish the analysis of the conductance-based integrate-and-fire neuron, we look at the stationary probability distributions with and without the effective time-constant approximation (figure 12). Top row corresponds to the parameters of the blue curve of

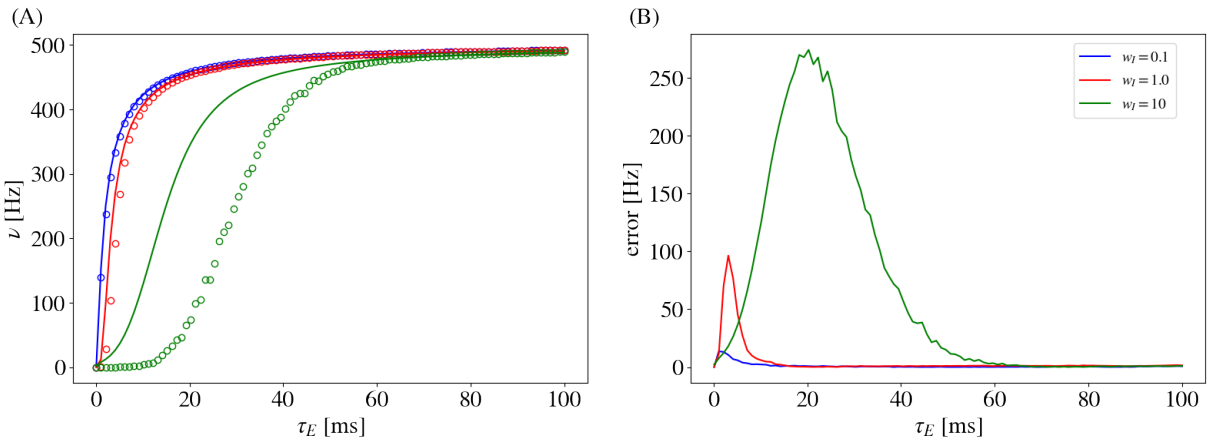


Figure 11 – Comparison of the analytical model with simulations for the simple conductance-based integrate-and-fire neuron using the full-multiplicative model. Three values of inhibitory synaptic weight were tested. (A) Firing rate and (B) absolute error between the the analytical firing rate and simulations. Relevant parameters are $w_E = 0.5$, $\nu_i = 5Hz$.

figure 8 and 10. Bottom corresponds to green curve in 9 and 11. It can be seen that better agreement is obtained for low (first column) and high (last column) $\tau_E$. For the transition region (middle column) agreement tends to be worst, especially in the high inhibition case (12E). This is to be expected since it is the region where the analytical firing rate also is not in good accord with data. The overestimation of the firing rate means that a larger amount of the distribution will be refractory, as observed by the smaller area under the curves.

It is also important to reinforce that using the effective time-constant approximation can provide better results in some situations but worst in others. The most explicit comparison case is figures 12C and 12D. In 12C, the approximation provides a better description of the distribution, while the full multiplicative model overestimates the left tail. The reverse happens for 12F, where the multiplicative model better accounts for both ends of the distribution.

## 3.2 Interpolated Integrate-and-Fire

A natural progression in the models to test is the addition of one mode channel to the neuron. More specifically, we will interpolate two excitatory channels with a proportion variable and keep the inhibitory the same. The excitatory channels can be classified as fast response and slow response channels. We write the model as

$$\tau_L \frac{dV}{dt} = -(V - E_L) - (1-\alpha) g_F(t)(V - E_E) - \alpha g_S(t)(V - E_E) - g_I(t)(V - E_I)\,, \quad (3.2.0.1)$$

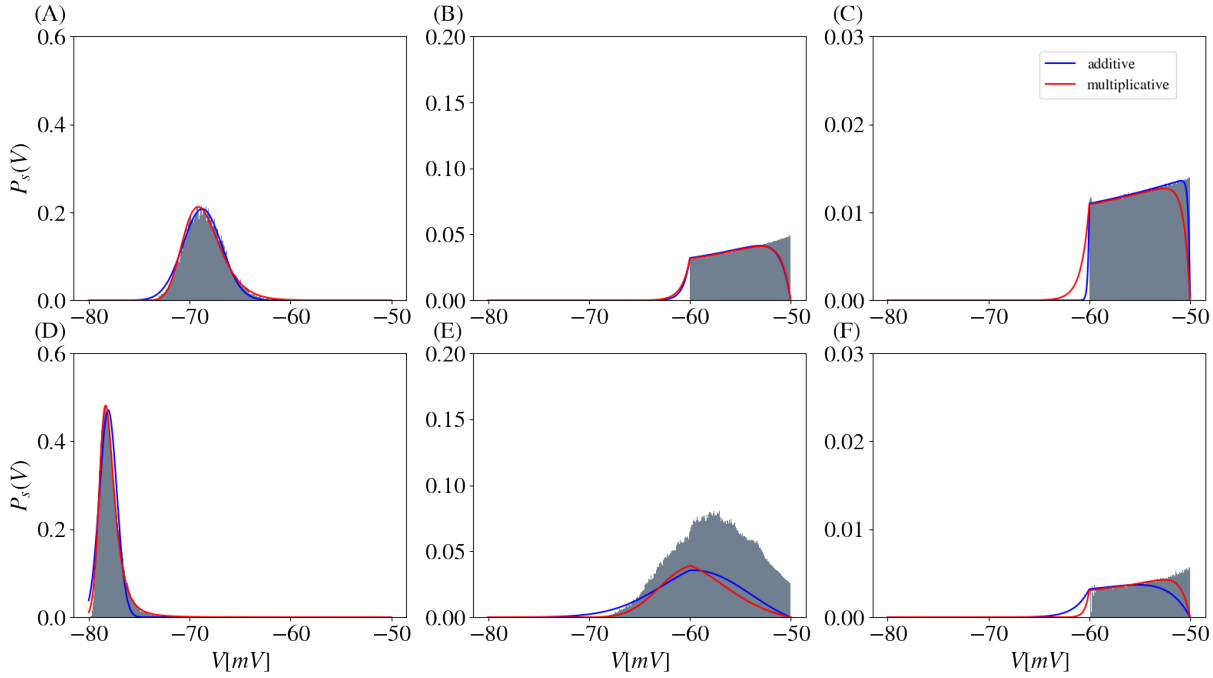


Figure 12 – Stationary probability distribution for conductance-based integrate-and-fire neuron. (A) $\tau_E = 1ms$, $w_E = 0.1$ and $w_I = 0.4$. (B) $\tau_E = 20ms$, $w_E = 0.1$ and $w_I = 0.4$. (C) $\tau_E = 70ms$, $w_E = 0.1$ and $w_I = 0.4$. (D) $\tau_E = 1ms$, $w_E = 0.5$ and $w_I = 10.0$. (E) $\tau_E = 20ms$, $w_E = 0.5$ and $w_I = 10.0$. (F) $\tau_E = 70ms$, $w_E = 0.5$ and $w_I = 10.0$. Additive model corresponds to the use of the effective time constant approximation, while multiplicative uses the full Langevin. Data for the grey histogram was collected from simulations over a period of 20s. Refractory time not displayed.

$$\tau_F \frac{dg_F}{dt} = -g_F + \sum_{j,k} w_E \delta(t - t_j^k)\,, \tag{3.2.0.2}$$

$$\tau_S \frac{dg_S}{dt} = -g_S + \sum_{j,k} w_E \delta(t - t_j^k)\,, \tag{3.2.0.3}$$

$$\tau_I \frac{dg_I}{dt} = -g_I + \sum_{j,k} w_I \delta(t - t_j^k)\,, \tag{3.2.0.4}$$

where $g_F$ is the fast conductance, $g_S$ is the slow conductance, and $\alpha$ indicates the proportion of fast and slow response channels. To keep this interpretation of the variable $\alpha$, we set $K_F = K_S = K_E$, $K_E$ the total number of excitatory input. The input firing rate for all populations $\nu_i$ is again kept constant. The values of the parameters of the interpolated conductance-based integrate-and-fire neuron are listed in table 2.

With this knowledge, the Langevin equation is written as

$$\frac{dV}{dt} = \frac{(V - \mu)}{\tau} + h_F(V)\eta_F(t) + h_S(V)\eta_S(t) + h_I(V)\eta_I(t)\,, \tag{3.2.0.5}$$

| Variable | Value |
|---|---|
| $\alpha$ | variable |
| $E_L$ | -60mV |
| $E_E$ | 0mV |
| $E_I$ | -80mV |
| $w_E$ | {0.1, 0.5} |
| $w_I$ | {0.1, 0.4, 1.0, 10.0} |
| $\tau_L$ | 20ms |
| $\tau_F$ | 1ms |
| $\tau_S$ | 100ms |
| $\tau_I$ | 10ms |
| $\tau_R$ | 2ms |
| $K_E$ | 400 |
| $K_I$ | 100 |
| $\theta$ | -50mV |
| $V_r$ | -60mV |
| $\nu_i$ | {5, 20, 50}Hz |

Table 2 – Table containing the set of parameters used for the interpolated conductance-based integrate-and-fire model.

where

$$\tau = \frac{\tau_L}{1 + (1-\alpha)\mu_F + \alpha\mu_S + \mu_I} \tag{3.2.0.6}$$

$$\mu = \frac{\tau}{\tau_L}(E_L + (1-\alpha)\mu_F E_E + \alpha\mu_S E_E + \mu_I E_I)\,, \tag{3.2.0.7}$$

$$h_F(V) = (1-\alpha)\frac{\sqrt{\tau_F}}{\tau_L}\sigma_F(E_E - V) \qquad h_S(V) = \alpha\frac{\sqrt{\tau_S}}{\tau_L}\sigma_S(E_E - V)\,, \tag{3.2.0.8}$$

$$h_I(V) = \frac{\sqrt{\tau_I}}{\tau_L}\sigma_I(E_I - V)\,. \tag{3.2.0.9}$$

Lets again compare the results of the method using the effective time-constant approximation and the full multiplicative Langevin.

### 3.2.1 Additive Noise

Application of the effective time-constant approximation results in

$$\frac{dV}{dt} = \frac{(V-\mu)}{\tau} + h_F\eta_F(t) + h_S\eta_S(t) + h_I\eta(t)\,, \tag{3.2.1.1}$$

where the coefficients are as earlier $h_F = h_F(\mu)$, $h_S = h_S(\mu)$, and $h_I = h_I(\mu)$. The Fox theory gives us again a transfer function with the same form as (2.2.5.5) and a stationary probability distribution (2.2.4.15), but now $\sigma_V$ is given by

$$\sigma_V^2 = \frac{\tau^2}{\tau+\tau_F}h_F^2 + \frac{\tau^2}{\tau+\tau_S}h_S^2 + \frac{\tau^2}{\tau+\tau_I}h_I^2\,. \tag{3.2.1.2}$$

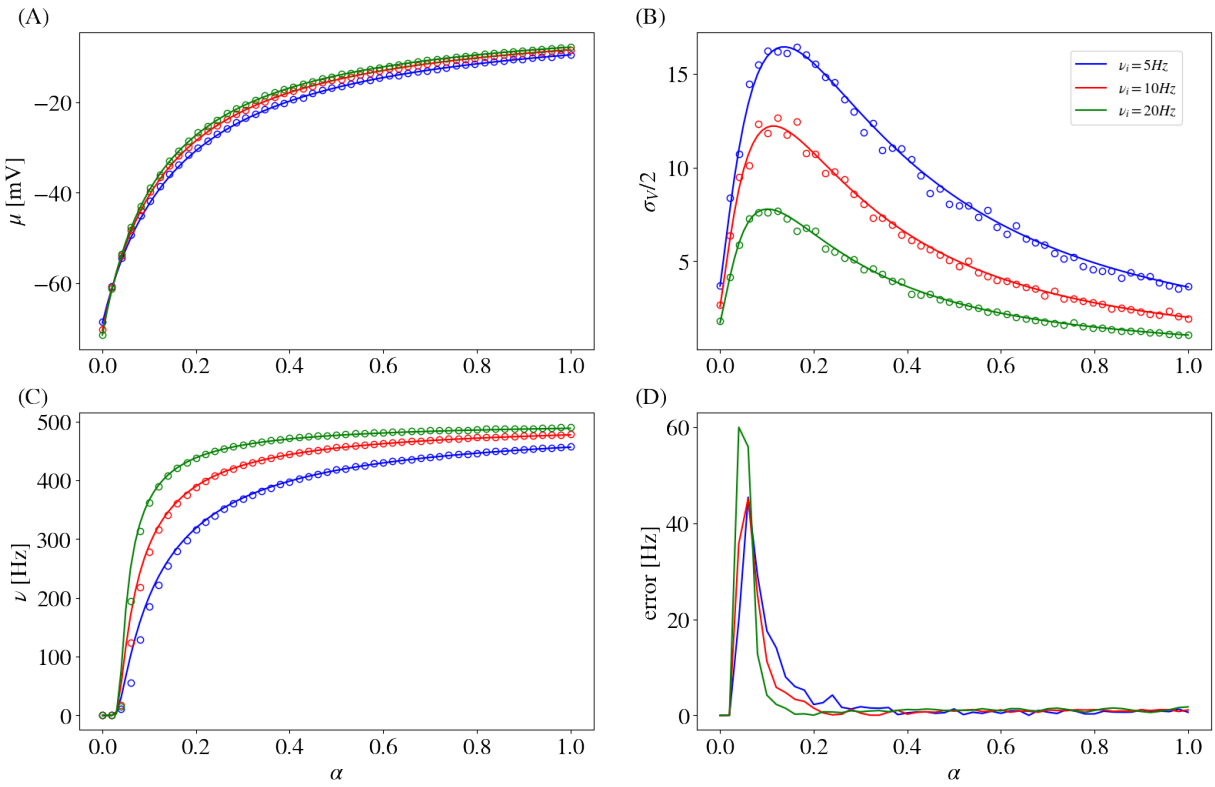


Figure 13 – Comparison of the analytical model with simulations for the interpolated neuron using the effective time-constant approximation. Three different values of input firing rate $\nu_i$ was used. (A) Mean potential for a thresholdless model. (B) Standard deviation of the membrane potential for the same thresholdless model. (C) Firing rate and (D) absolute error between the the analytical firing rate and simulations. Relevant parameters are $w_E = 0.1$, $w_I = 0.4$.

Comparing the resulting mean potential and the standard deviation for the thresholdless model we see, again, good agreement for all values (figure 13). We can also see that the mean potential is the same as in the simple conductance-based integrate-and-fire neuron. This equivalence can be explicit calculated by using $\tau_E = (1 - \alpha)\tau_F + \alpha\tau_S$ in the expression of $\mu$. However, the equivalence doesn't occur for the standard deviation, which has a less pronounced maximum in the interpolated case. The transfer function retains an almost identical shape to the conductance-based, which means that what contributes the most in the form of the curve is the mean potential. In any case, the error continues to be small except for the small transition region.

We can now proceed to change the inhibition levels by modifying $w_I$. As expected, the mean potential behaves the same as in the simple conductance-based neuron. The standard deviation presents a more pronounced difference, not only changing the peak values but also changing the overall shape of the curve. Specifically, the interpolated model exhibits smaller values in general and the curve for $w_I = 0.1$ decreases monotonically. The analytical transfer function doesn't work very well again for $w_I = 10$. The transition

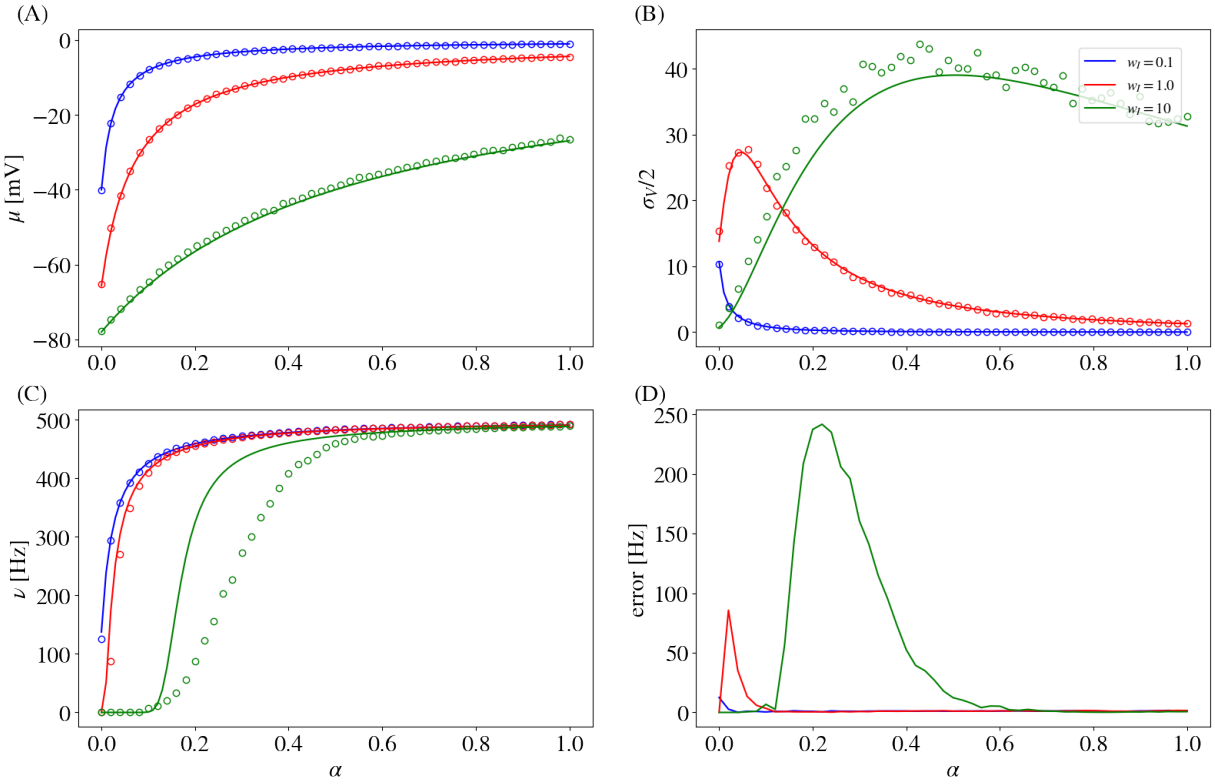


Figure 14 – Comparison of the analytical model with simulations for the interpolated neuron using the effective time-constant approximation. Three different values of inhibitory synaptic weight was used. (A) Mean potential for a threshold-less model. (B) Standard deviation of the membrane potential for the same thresholdless model. (C) Firing rate and (D) absolute error between the the analytical firing rate and simulations. Relevant parameters are $w_E = 0.5$, $\nu_i = 5Hz$.

is again exceedingly sharper than expected. Let's again look at the treatment of the full-multiplicative model.

### 3.2.2 Multiplicative Noise

The Fokker-Planck for the multiplicative model has now three diffusion terms, the fast and the slow excitatory ones, and the same inhibitory one. The form of the equation is therefore

$$\frac{\partial P}{\partial t} = -\frac{\partial}{\partial V}\left[W(V)P\right] + \frac{\partial}{\partial V}h_F(V)\frac{\partial}{\partial V}(S_F(V)P) + \frac{\partial}{\partial V}h_S(V)\frac{\partial}{\partial V}(S_S(V)P) + \frac{\partial}{\partial V}h_I(V)\frac{\partial}{\partial V}(S_I(V)P)\,, \tag{3.2.2.1}$$

where again the functions $S_F(V)$, $S_S(V)$, and $S_I(V)$ can be inferred from the generic expression (2.2.6.3). We obtain the same linear differential equation

$$\frac{\partial P_s}{\partial V} + B(V)P_s = -\nu H(V)\,, \tag{3.2.2.2}$$

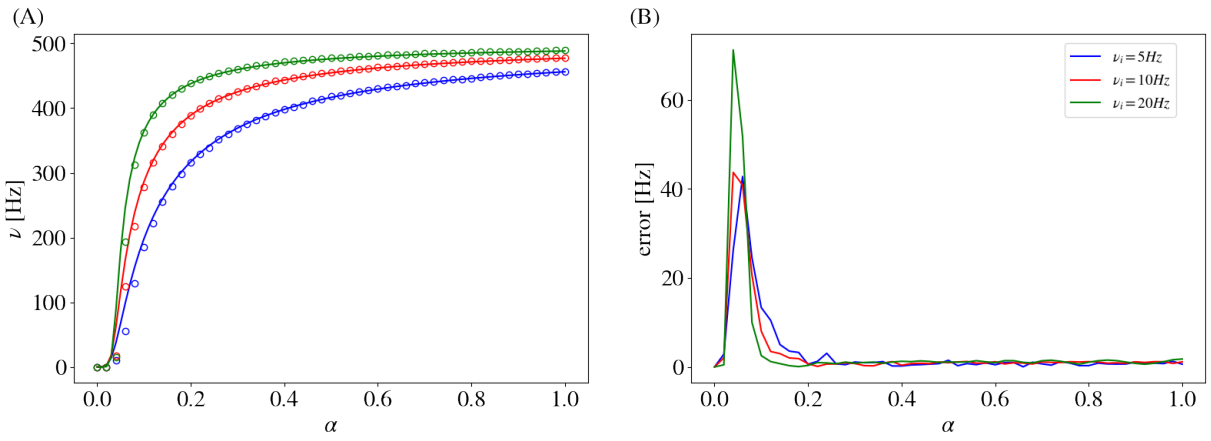


Figure 15 – Comparison of the interpolated model with simulations for three different values of input firing rate $\nu_i$ as a function of the interpolation parameter $\alpha$. Full multiplicative model was used testing for three values of input rate. (A) Mean potential for a thresholdless model. (B) Standard deviation of the membrane potential for the same thresholdless model. (C) Firing rate and (D) absolute error between the the analytical firing rate and simulations. Relevant parameters are $w_E = 0.1$, $w_I = 0.4$.

with coefficients

$$B(V) = \frac{h_F(V)S'_F(V) + h_S(V)S'_S(V) + h_I(V)S'_I(V) - W(V)}{\chi(V)}\,, \tag{3.2.2.3}$$

$$H(V) = \frac{\Theta(V - V_r)}{\chi(V)}\,, \tag{3.2.2.4}$$

$$\chi(V) = h_F(V)S_F(V) + h_S(V)S_S(V) + h_I(V)S_I(V)\,. \tag{3.2.2.5}$$

Looking at figures 15 and 16, the behavior of the simple conductance base repeats here, with the multiplicative model exhibiting a smoother transitions but with an early beginning. It is, again, heavily implied by the figures that a translation in the $\alpha$ direction would improve the results dramatically in the high inhibition case. A deeper investigation of this behavior and how generalizable it is for other parameters and neuron models is needed.

It is clear that the behavior of the simple conductance-based integrate-and-fire and the interpolated one is essentially the same at least when we are considering the firing rate. The small deviations in the variance of the noise don't translate into significant differences in how the neuron fires when receiving a stationary input.

The comparison of the stationary probability distributions tells us again that using the effective time-constant approximation or not doesn't guarantee a better result (figure 17). Even though the full-multiplicative model gives us a better description of the distribution for most of the cases in the picture, for 17C the approximation better

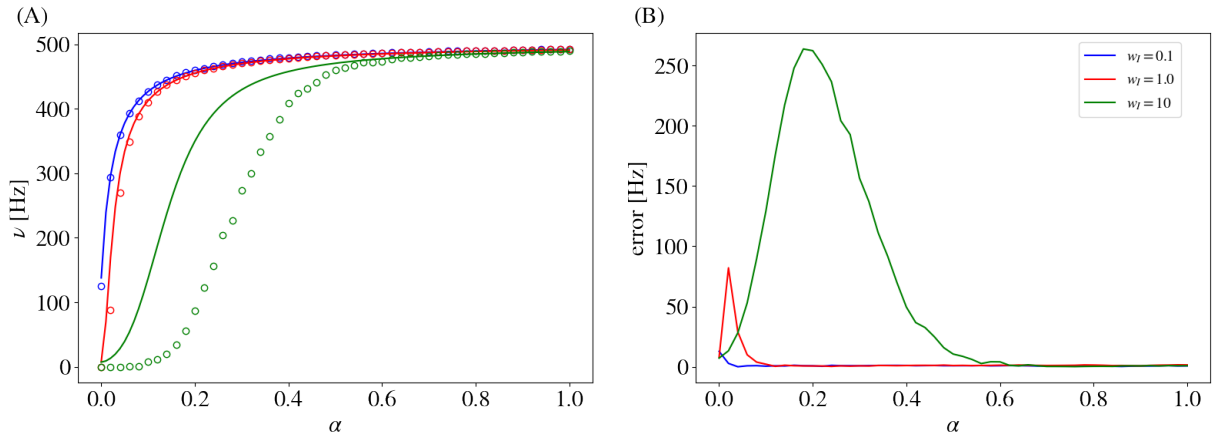


Figure 16 – Comparison of the interpolated analytical model with simulations for three different values of inhibitory synaptic weight $w_I$ as a function of the interpolation parameter $\alpha$. Full multiplicative model was used testing for three values of inhibitory synaptic weight.(A) Mean potential for a thresholdless model. (B) Standard deviation of the membrane potential for the same thresholdless model. (C) Firing rate and (D) absolute error between the the analytical firing rate and simulations. Relevant parameters are $w_E = 0.5$, $\nu_i = 5Hz$.

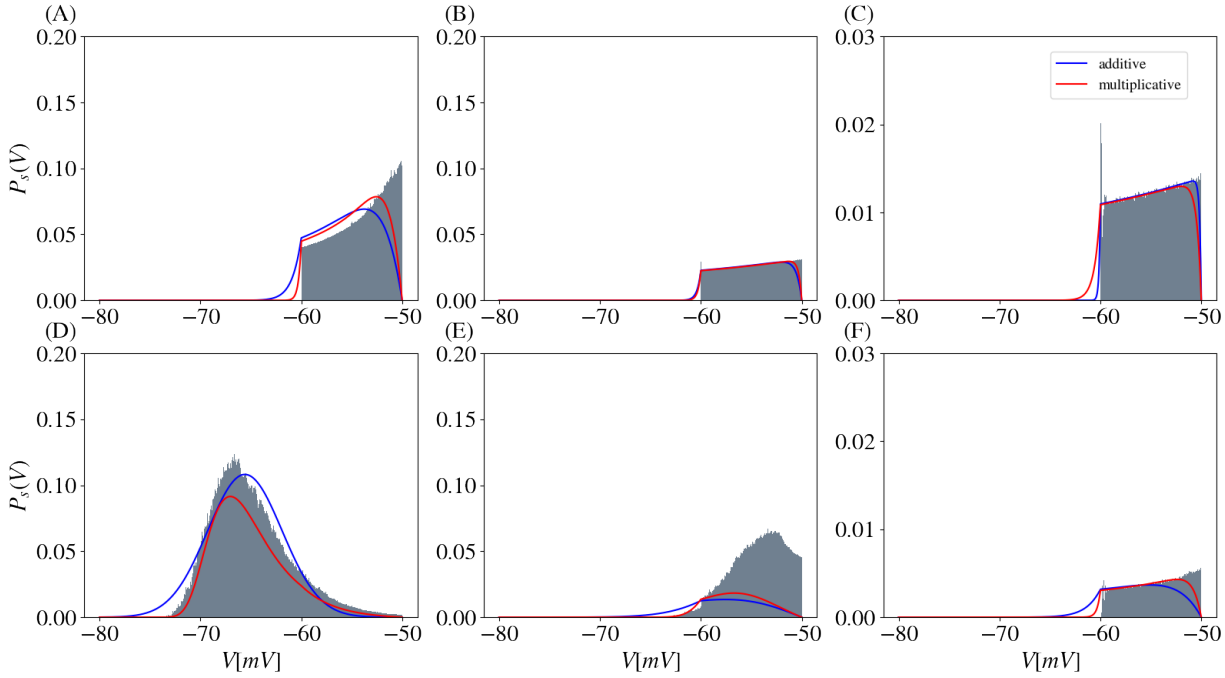


Figure 17 – Stationary probability distribution for different parameters of the interpolated model. (A) $\alpha = 0.1$, $w_E = 0.1$ and $w_I = 0.4$. (B) $\alpha = 0.3$, $w_E = 0.1$ and $w_I = 0.4$. (C) $\alpha = 0.7$, $w_E = 0.1$ and $w_I = 0.4$. (D) $\alpha = 0.1$, $w_E = 0.5$ and $w_I = 10.0$. (E) $\alpha = 0.3$, $w_E = 0.5$ and $w_I = 10.0$. (F) $\alpha = 0.7$, $w_E = 0.5$ and $w_I = 10.0$. Additive model corresponds to the use of the effective time constant approximation, while multiplicative uses the full Langevin. Data for the grey histogram was collected from simulations over a period of 20s. Refractory time not displayed.

encapsulate the data. For the transition region in the high inhibition case we can see that the analytical result is considerably flatter than the real distribution and has a smaller area. This is to be expected since it overestimates the firing rate and therefore a larger portion of the distribution is refractory.

## 3.3 NMDA Integrate-and-Fire

Until now, there was no $V$ nonlinearity in the resulting Langevin equation of the neurons tested. In principle, our mean-field method should be able to deal with nonlinearities in the drift term, in the diffusion terms, or both. Here we will add a nonlinearity by introducing NMDA channels. NMDA channels are excitatory channels that the activation depends also on the membrane potential, as stated in the introduction. An appropriate way to model this behavior is by adding an appropriately tuned sigmoidal factor to the conductance term (JAHR; STEVENS, 1990). The complete model can be written as

$$\tau_L \frac{dV}{dt} = -(V-E_L)-(1-\alpha)g_A(t)(V-E_E)-\alpha s(V)g_N(t)(V-E_E)-g_I(t)(V-E_I)\,, \quad (3.3.0.1)$$

$$\tau_A \frac{dg_A}{dt} = -g_A + \sum_{j,k} w_E \delta(t-t_j^k)\,, \quad (3.3.0.2)$$

$$\tau_N \frac{dg_N}{dt} = -g_N + \sum_{j,k} w_E \delta(t-t_j^k)\,, \quad (3.3.0.3)$$

$$\tau_I \frac{dg_I}{dt} = -g_I + \sum_{j,k} w_I \delta(t-t_j^k)\,, \quad (3.3.0.4)$$

$$s(V) = \frac{1}{1+([\mathrm{Mg}^{2+}]/\gamma)\exp(-\beta V)}\,, \quad (3.3.0.5)$$

where $g_A$ are the AMPA channels (excitatory fast acting channels here), $g_N$ the NMDA channels, $s$ is the sigmoidal modulating function, $[\mathrm{Mg}^{2+}]$ is the concentration of magnesium ions, and $\gamma$ and $\beta$ are fitting parameters. For $\alpha$ to represent the proportion of AMPA and NMDA channels, we again keep the number of their inputs equal, i.e, $K_A = K_N = K_E$, and $K_E$ the number of excitatory inputs. The input rate $\nu_i$ is also the same for all populations. The list of the parameters and their values are kept in table 3.

The set of equations for this model when applied the diffusion approximation and reduced to a one dimensional Langevin equation produces

$$\frac{dV}{dt} = \frac{(V-\mu(V))}{\tau(V)} + h_A(V)\eta_A(t) + h_N(V)\eta_N(t) + h_I(V)\eta_I(t)\,, \quad (3.3.0.6)$$

where

$$\tau(V) = \frac{\tau_L}{1+(1-\alpha)\mu_A + \alpha s(V)\mu_N + \mu_I} \quad (3.3.0.7)$$

| Variable | Value |
|---|---|
| $\alpha$ | variable |
| $E_L$ | -60mV |
| $E_E$ | 0mV |
| $E_I$ | -80mV |
| $w_E$ | {0.1, 0.5} |
| $w_I$ | {0.1, 0.4, 1.0, 10.0} |
| $\tau_L$ | 20ms |
| $\tau_A$ | 1ms |
| $\tau_N$ | 100ms |
| $\tau_I$ | 10ms |
| $\tau_R$ | 2ms |
| $K_E$ | 400 |
| $K_I$ | 100 |
| $\theta$ | -50mV |
| $V_r$ | -60mV |
| $\nu_i$ | {5, 20, 50}Hz |
| $[Mg^{2+}]$ | 1mM |
| $\gamma$ | 3.57mM |
| $\beta$ | $0.062(\text{mV})^{-1}$ |

Table 3 – Table containing the set of parameters used for the interpolated conductance based integrate and fire model.

$$\mu(V) = \frac{\tau}{\tau_L}(E_L + (1-\alpha)\mu_A E_E + \alpha s(V)\mu_N E_E + \mu_I E_I)\,, \tag{3.3.0.8}$$

$$h_A(V) = (1-\alpha)\frac{\sqrt{\tau_A}}{\tau_L}\sigma_A(E_E - V) \qquad h_N(V) = \alpha s(V)\frac{\sqrt{\tau_N}}{\tau_L}\sigma_N(E_E - V)\,, \tag{3.3.0.9}$$

$$h_I(V) = \frac{\sqrt{\tau_I}}{\tau_L}\sigma_I(E_I - V)\,. \tag{3.3.0.10}$$

It is clear now that we can't use the effective time-constant approximation to obtain a coherent result. The term $h_N(V)$ is no longer linear, and the approximation loses its logic [Richardson,Gerstner:2005]. We also have a highly nonlinear drift term, as the effective membrane time-constant $\tau(V)$ and the stationary potential $\mu(V)$ depends on the membrane potential $V$ through the modulating function $s(V)$. It is possible to modify the equation (3.3.0.1) so that the effective time-constant approximation becomes applicable again. To this end it is necessary to linearize the term $s(V)(V - E_E)$ around the average membrane potential value $\langle V \rangle$, so that all terms are linear in $V$ again. This procedure was used by Brunel and Wang to see the effects of NMDA neuromodulation on working memory (BRUNEL; WANG, 2001). The disadvantage of this method is that it introduce the firing rate itself in the Langevin, needing a self consistent procedure to get the resulting

firing rate. Therefore, we will not use the approximation, treating the full-model, since our method don't have any restrictions of this kind.

Calculating the Fokker-Planck, we get the following

$$\frac{\partial P}{\partial t} = -\frac{\partial}{\partial V}\left[W(V)P\right] + \frac{\partial}{\partial V}h_A(V)\frac{\partial}{\partial V}(S_A(V)P) + \frac{\partial}{\partial V}h_N(V)\frac{\partial}{\partial V}(S_N(V)P) + \frac{\partial}{\partial V}h_I(V)\frac{\partial}{\partial V}(S_I(V)P)\,, \tag{3.3.0.11}$$

where the functions $S_A(V)$, $S_N(V)$, and $S_I(V)$ are given by (2.2.6.3). We also note that $W(V)$ is no longer linear in $V$ and will result in different functional forms for the $S$ functions. The linear differential equation in $V$ is then

$$\frac{\partial P_s}{\partial V} + B(V)P_s = -\nu H(V)\,, \tag{3.3.0.12}$$

with coefficients

$$B(V) = \frac{h_A(V)S'_A(V) + h_N(V)S'_N(V) + h_I(V)S'_I(V) - W(V)}{\chi(V)}\,, \tag{3.3.0.13}$$

$$H(V) = \frac{\Theta(V - V_r)}{\chi(V)}\,, \tag{3.3.0.14}$$

$$\chi(V) = h_A(V)S_A(V) + h_N(V)S_N(V) + h_I(V)S_I(V)\,. \tag{3.3.0.15}$$

We proceed to test this model against simulation data for different input rates (figure 18A and 18B) and for different inhibitory weights (figure 18C and 18D). Given the highly nonlinear model in hands, it is remarkable how good the agreement between the mean-field result and the simulations iss for the majority of the cases. We can see the early rise of the curve as in the previous models, so the method retains, even in this case, the overestimation of the firing rate. But it is notable that a slight translation in the $\alpha$ axis can result in a better fitting, similar to our previous results for the full-multiplicative model. The only case where the model isn't a good descriptor is for $w_I = 10$. In this case the early rise of the curve is really pronounced when the simulation data barely moves.

There is also a crucial point that we need to allude to. In the methods, we imposed the condition for uniform convergence (2.2.4.22) as a metric for the good behavior of the method (FOX, 1986b). In the linear conductance-based models, this condition was obeyed for all values. However, the introduction of the NMDA nonlinearity makes this condition break for a large range of parameters. This is the case for the curves in figure 18C. Notably, breaking this condition didn't affect the ability of the model to describe the system. But, for the method to work correctly it is necessary to deal with the divergence point at $1 - \tau_i\left(W'(y) - \frac{h'_i(y)}{h_i(y)}W(y)\right) = 0$. For a lack of time, we removed the divergences by removing the diverging values of $B$ and $H$ when numerically integrating. This resulted in some kinks and distortions in the results of figure 18C, but is clear that a more clever procedure can completely remove these instabilities without compromising the model.

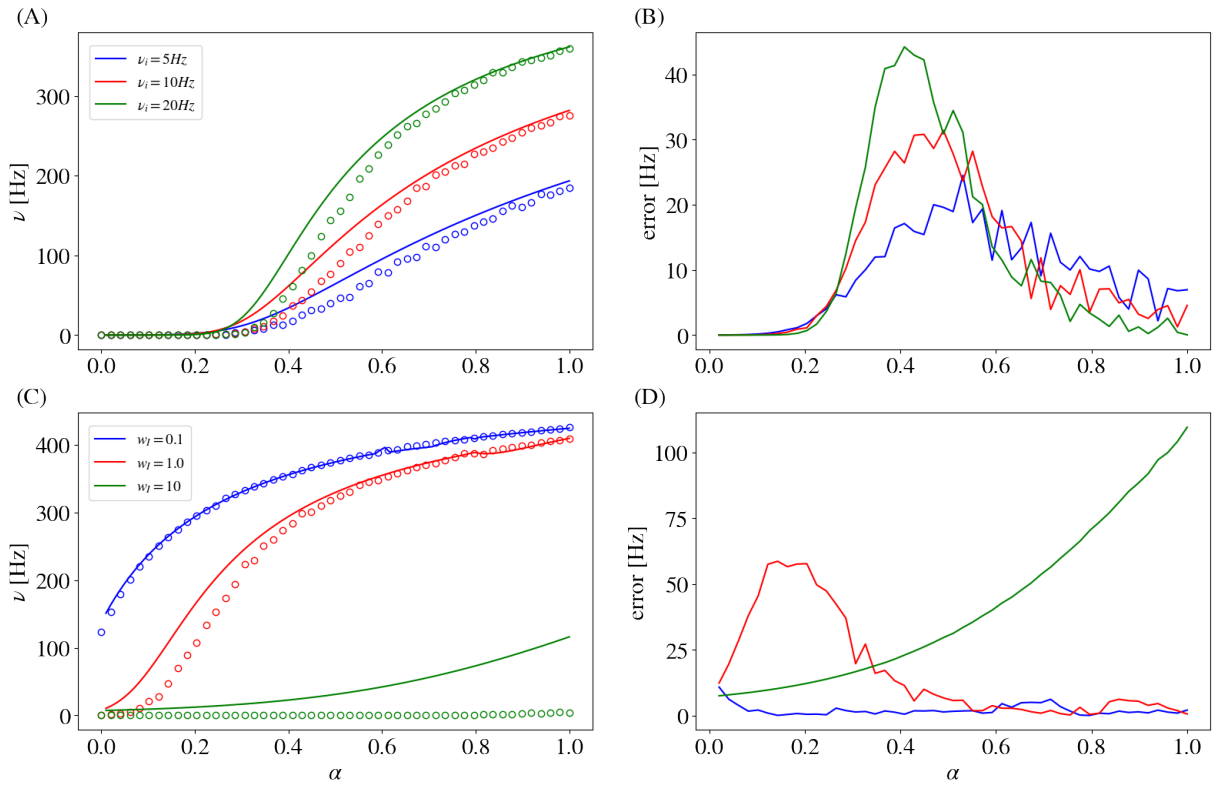


Figure 18 – Comparison of the NMDA analytical model with simulations for three different values of input rate $\nu_I$ and inhibitory synaptic weight $w_I$ as a function of the interpolation parameter $\alpha$. (A) Firing rate and (B) error of the analytical model for the different input rates with $w_E = 0.1$ and $w_I = 0.4$. (C) Firing rate and (D) absolute error between the the analytical firing rate and simulations for three values of inhibitory weights $w_I$ with $w_E = 0.5$ and $\nu_i = 5$Hz

Lastly, we can look at the probability distributions estimated for the NMDA model (figure 19). For the top row, the estimation is good when the distribution don't interact heavily with the threshold but degrades when this interaction is significant. On the bottom row, where $w_I = 10$, the estimation works really well for all values of $\alpha$. This happens for the same reason as the figure 19A, that is, the distribution is concentrated well bellow the threshold, and for this reason the absorbing barrier have little effect in the model.

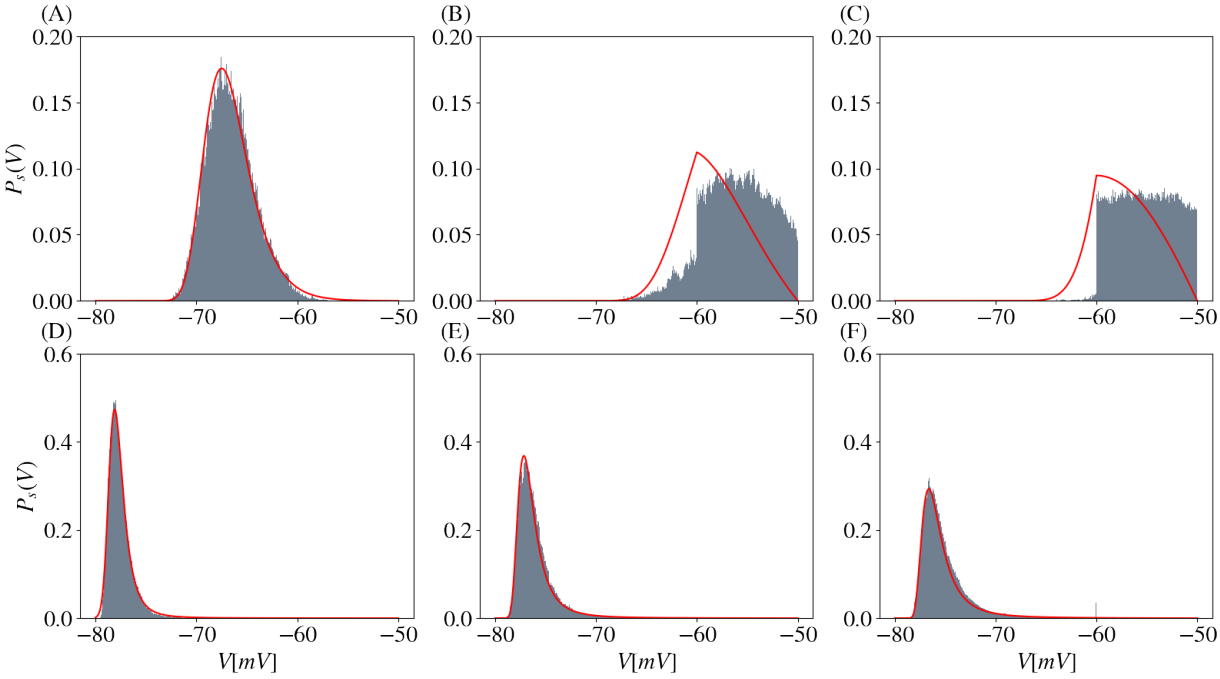


Figure 19 – Stationary probability distribution for the NMDA model with different parameters. (A) $\alpha = 0.1$, $w_E = 0.1$ and $w_I = 0.4$. (B) $\alpha = 0.5$, $w_E = 0.1$ and $w_I = 0.4$. (C) $\alpha = 0.7$, $w_E = 0.1$ and $w_I = 0.4$. (D) $\alpha = 0.1$, $w_E = 0.5$ and $w_I = 10.0$. (E) $\alpha = 0.5$, $w_E = 0.5$ and $w_I = 10.0$. (F) $\alpha = 0.7$, $w_E = 0.5$ and $w_I = 10.0$. Red curve corresponds to the probability distribution estimated from the model. Data for the grey histogram was collected from simulations over a period of 20s. Refractory time not displayed.

# 4 Conclusion

In this work, we have developed a new method for the construction of a transfer function that gives the firing rate of a generic conductance-based integrate-and-fire neuron. The method is based on the standard diffusion approximation, which substitutes the Poissonian input with a gaussian white noise with the same mean and variance as the original. We reduced the N-dimensional system into a single Langevin equation with colored and multiplicative noise, which does not have a corresponding exact Fokker-Planck equation. To solve this problem, we used an extension of the Fox theory [Fox, 1986A-1986B] to construct an effective Fokker-Planck equation, which can be used to obtain the resulting stationary firing rate. Three distinct neuron models with progressive complexity were picked to test the method described, namely, a standard conductance-based integrate-and-fire; an interpolated fast and slow channels conductance-based integrate-and-fire; and a conductance-based integrate-and-fire with nonlinear NMDA channels.

The mean-field result for the standard conductance-based integrate-and-fire neuron was compared with the firing rate data resulting from simulations as a function of the excitatory time constant. We also compared the use of the effective time-constant approximation, which reduces the linear multiplicative terms into additive ones, to the full treatment of the multiplicative Langevin. We saw good agreement between the data and the mean-field results in most of the scenarios tested. The only exception was for the high inhibition case, where the error was considerably high for the transition region. A quick look at the stationary membrane potential for the thresholdless model tells us that the region of large error is the fluctuation-driven one, where spikes are generated by fluctuations in the membrane potential. The method, therefore, tends to overestimate the firing rate in this region. We can also see that, even though the error is smaller when we use the effective time-constant approximation, the qualitative behavior for the multiplicative model was better. The results for the multiplicative model also suggest that a translational correction can improve the results. Corrections with the form proposed by Brunel and Sergi (BRUNEL; SERGI, 1998) for the model with the effective time-constant approximation may be a fruitful way to get a better description of the data in some cases since it provides higher order terms in the fastest time constant channel. However, we did not manage to test this hypothesis in our models.

The interpolated integrate-and-fire model produced a very similar result as the standard one. That is mostly because the stationary membrane potential is the same in both models. The differences in the variance of the noise are not sufficient to significantly change the resulting firing rate. So in terms of the firing rate behavior, changing the proportion of fast and slow channels corresponds to changing the response time of one

single type of channel.

At last we added nonlinear NMDA channels to the model to teste the effectiveness of the method for nonlinear terms. The nonlinearity in the resulting diffusion coefficients required extra care, since for some set of parameters the system goes outside the range of validity of the method and divergences can occur. However, if the divergences are taken care in an appropriate manner, the method produces a good description of the simulated data even when outside the range of validity. The exception is again the region of high inhibition, where the method generates an early rising curve.

We also plotted the probability distributions of the membrane potential against the simulation data. It was noticeable that the probability distribution obtained from the method was a good approximation of the real distributions when the influence of the threshold was minor. That occurs when the average membrane potential is sufficient low, not generating spikes, or when it is high enough so that spikes are constant. When between these regions, the resulting probability distributions can result in lousy representations.

We stopped at this three types of neuron models. However, the method proposed here, in principle, goes beyond these three test cases. One of these extensions, mentioned in the methods section, is the possible introduction of the nonlinear term $\psi(V)$ in the drift expression. This nonlinear term can represent a quadratic (LATHAM et al., 2000) or an exponential integrate-and-fire neuron (FOURCAUD-TROCMÉ et al., 2003), for example. It is also possible to introduce adaptation currents that depends on the spiking time of the modeled neuron. This would introduce the firing rate in the resulting Langevin equation, making a self-consistent treatment required.

It is also possible to look for non-stationary solutions when the input changes in time. Let's say we introduce an oscillatory Poissonian input. It is possible to construct a Fokker-Planck equation with the Fox theory since the noise terms still have the same form but are now modulated by the firing rate. Nonetheless, only the stationary solutions of Fox theory are valid for all the range of the time constants (JUNG; HÄNGGI, 1987). The non-stationary ones are valid in the small $\tau_i$ limit, and careful consideration of this fact is necessary when putting the method into practice.

Finally, we allure to the fact that we can use this procedure to study networks of spiking neurons in equilibrium. If the neuron is inserted in a network of similar units, then it is expected that the resulting firing rate of this neuron is similar to the rest of the network. Effectively, this means that we can set the input rate as equal to the output rate for neurons of the same type, and solve it in a self-consistent manner (FENG, 2003). This was famously done by Brunel to evaluate phase transitions of a network of simple current based integrate and fire neurons (BRUNEL; BRUNEL, 2000). Stability and oscillations, however, can be a little challenging to calculate for some of the models given here, since the nonlinearities complicate the analysis.

# Bibliography

ADRIAN, E. D. A. *The Basis of Sensation: The Action of the Sense Organs*. [S.l.]: Christophers, 1928. Citado na página 24.

AGMON-SNIR, H.; CARR, C. E.; RINZEL, J. The role of dendrites in auditory coincidence detection. *Nature*, v. 393, n. 6682, p. 268–272, maio 1998. Citado na página 23.

AMIT, D. J.; BRUNEL, N. Model of global spontaneous activity and local structured activity during delay periods in the cerebral cortex. *Cereb. Cortex*, v. 7, n. 3, p. 237–252, 1997. Citado 2 vezes nas páginas 26 and 31.

BRESSLOFF, P. C. Spatiotemporal dynamics of continuum neural fields. *J. Phys. A: Math. Theor.*, IOP Publishing, v. 45, n. 3, p. 033001, dez. 2011. Citado na página 19.

BRUNEL, N.; BRUNEL, N. Dynamics of sparsely connected networls of excitatory and inhibitory neurons. *Computational Neuroscience*, v. 8, p. 183–208, 2000. Citado na página 62.

BRUNEL, N. et al. Effects of synaptic noise and filtering on the frequency response of spiking neurons. *Phys. Rev. Lett.*, American Physical Society (APS), v. 86, n. 10, p. 2186–2189, mar. 2001. Citado na página 27.

BRUNEL, N.; LATHAM, P. E. Firing rate of the noisy quadratic integrate-and-fire neuron. *Neural Comput.*, v. 15, n. 10, p. 2281–2306, out. 2003. Citado na página 29.

BRUNEL, N.; SERGI, S. Firing frequency of leaky intergrate-and-fire neurons with synaptic current dynamics. *J. Theor. Biol.*, v. 195, n. 1, p. 87–95, nov. 1998. Citado 3 vezes nas páginas 19, 28, and 61.

BRUNEL, N.; WANG, X. J. Effects of neuromodulation in a cortical network model of object working memory dominated by recurrent inhibition. *J. Comput. Neurosci.*, v. 11, n. 1, p. 63–85, jul. 2001. Citado na página 57.

BUONOMANO, D. V.; MAASS, W. State-dependent computations: spatiotemporal processing in cortical networks. *Nat. Rev. Neurosci.*, v. 10, n. 2, p. 113–125, 2009. Citado na página 23.

CAMERA, G. L. The mean field approach for populations of spiking neurons. set. 2021. Citado na página 19.

DAYAN, P.; ABBOTT, L. F. *Theoretical Neuroscience: Computational and Mathematical Modeling of Neural Systems*. [S.l.]: MIT Press, 2005. Citado 2 vezes nas páginas 20 and 23.

ERMENTROUT, B. Neural networks as spatio-temporal pattern-forming systems. *Rep. Prog. Phys.*, IOP Publishing, v. 61, n. 4, p. 353, abr. 1998. Citado na página 25.

FENG, J. *Computational Neuroscience: A Comprehensive Approach*. [S.l.]: CRC Press, 2003. Citado 3 vezes nas páginas 26, 31, and 62.

FOURCAUD-TROCMÉ, N. et al. How spike generation mechanisms determine the neuronal response to fluctuating inputs. *J. Neurosci.*, v. 23, n. 37, p. 11628–11640, dez. 2003. Citado 2 vezes nas páginas 27 and 62.

FOX, R. F. Functional-calculus approach to stochastic differential equations. *Phys. Rev. A Gen. Phys.*, APS, v. 33, n. 1, p. 467–476, jan. 1986. Citado 2 vezes nas páginas 34 and 37.

FOX, R. F. Uniform convergence to an effective Fokker-Planck equation for weakly colored noise. *Phys. Rev. A Gen. Phys.*, APS, v. 34, n. 5, p. 4525–4527, nov. 1986. Citado 3 vezes nas páginas 34, 38, and 58.

GERSTEIN, G. L.; MANDELBROT, B. Random walk models for the spike activity of a single neuron. *Biophys. J.*, v. 4, p. 41–68, jan. 1964. Citado na página 26.

GERSTNER, W. et al. *Neuronal dynamics: From single neurons to networks and models of cognition*. Cambridge, England: Cambridge University Press, 2014. Citado na página 25.

GLOVER, G. H. Overview of functional magnetic resonance imaging. *Neurosurg. Clin. N. Am.*, v. 22, n. 2, p. 133–9, vii, abr. 2011. Citado na página 19.

GRIGOLINI, P. et al. Fokker-Planck description of stochastic processes with colored noise. *Phys. Rev. A Gen. Phys.*, v. 38, n. 4, p. 1966–1978, ago. 1988. Citado 2 vezes nas páginas 34 and 38.

HAHNLOSER, R. H. R.; KOZHEVNIKOV, A. a.; FEE, M. S. An ultra-sparse code underlies the generation of neural sequences in a songbird. *Nature*, v. 419, n. 6902, p. 65–70, 2002. Citado na página 23.

IZHIKEVICH, E. M. *Dynamical Systems in Neuroscience*. [S.l.]: MIT Press, 2007. Citado na página 20.

JAHR, C. E.; STEVENS, C. F. Voltage dependence of NMDA-activated macroscopic conductances predicted by single-channel kinetics. *J. Neurosci.*, v. 10, n. 9, p. 3178–3182, set. 1990. Citado na página 56.

JUNG, P.; HÄNGGI, P. Dynamical systems: A unified colored-noise approximation. *Phys. Rev. A Gen. Phys.*, v. 35, n. 10, p. 4464–4466, maio 1987. Citado 3 vezes nas páginas 34, 38, and 62.

KOZIOL, L. F. et al. Structure and function of large-scale brain systems. *Appl. Neuropsychol. Child*, v. 3, n. 4, p. 236–244, 2014. Citado na página 19.

LAJE, R.; BUONOMANO, D. V. Robust timing and motor patterns by taming chaos in recurrent neural networks. *Nat. Neurosci.*, v. 16, n. 7, p. 925–933, 2013. Citado na página 23.

LATHAM, P. E. et al. Intrinsic dynamics in neuronal networks. i. theory. *J. Neurophysiol.*, v. 83, n. 2, p. 808–827, fev. 2000. Citado na página 62.

LINDENBERG, K.; WEST, B. J. Finite correlation time effects in nonequilibrium phase transitions. *Physica A*, Elsevier BV, v. 119, n. 3, p. 485–503, maio 1983. Citado na página 34.

LUBOEINSKI, J.; TETZLAFF, C. Organization and priming of long-term memory representations with two-phase plasticity. *Cognit. Comput.*, jun. 2022. Citado na página 24.

MILLER, E. K. The prefrontal cortex: complex neural properties for complex behavior. *Neuron*, v. 22, n. 1, p. 15–17, jan. 1999. Citado na página 23.

MOLTER, C.; COLLIAUX, D.; YAMAGUCHI, Y. Working memory and spontaneous activity of cell assemblies. a biologically motivated computational model. In: *2008 IEEE International Joint Conference on Neural Networks (IEEE World Congress on Computational Intelligence)*. [S.l.: s.n.], 2008. p. 3070–3077. Citado na página 24.

MOUNTCASTLE, V. B. The columnar organization of the neocortex. *Brain*, v. 120 ( Pt 4), p. 701–722, abr. 1997. Citado na página 24.

Nicolas Brunel; Vincent Hakim. Fast global oscillations in networks of Integrate-and-Fire neurons with low firing rates. *Neural Comput.*, v. 1671, p. 1621–1671, 1999. Citado na página 27.

NIEBUR, E. Neuronal cable theory. *Scholarpedia J.*, Scholarpedia, v. 3, n. 5, p. 2674, 2008. Citado na página 23.

NOBUKAWA, S. et al. Analysis of chaotic resonance in izhikevich neuron model. *PLoS One*, v. 10, n. 9, p. e0138919, set. 2015. Citado na página 23.

OBIEN, M. E. J. et al. Revealing neuronal function through microelectrode array recordings. *Front. Neurosci.*, v. 8, p. 423, 2014. Citado na página 19.

OSTOJIC, S.; BRUNEL, N. From spiking neuron models to linear-nonlinear models. *PLoS Comput. Biol.*, Public Library of Science (PLoS), v. 7, n. 1, p. e1001056, jan. 2011. Citado na página 19.

PAMPALONI, N. P. et al. Slow AMPA receptors in hippocampal principal cells. *Cell Rep.*, v. 36, n. 5, p. 109496, ago. 2021. Citado na página 22.

PURVES, D. et al. *Neurosciences*. [S.l.]: De Boeck Superieur, 2019. Citado na página 20.

RICHARDSON, M. J. E. Effects of synaptic conductance on the voltage distribution and firing rate of spiking neurons. *Phys. Rev. E Stat. Nonlin. Soft Matter Phys.*, American Physical Society (APS), v. 69, n. 5 Pt 1, p. 051918, maio 2004. Citado 2 vezes nas páginas 28 and 33.

RICHARDSON, M. J. E. Firing-rate response of linear and nonlinear integrate-and-fire neurons to modulated current-based and conductance-based synaptic drive. *Phys. Rev. E Stat. Nonlin. Soft Matter Phys.*, American Physical Society (APS), v. 76, n. 2 Pt 1, p. 021919, ago. 2007. Citado na página 29.

RICHARDSON, M. J. E.; GERSTNER, W. Synaptic shot noise and conductance fluctuations affect the membrane voltage with equal significance. *Neural Comput.*, v. 17, n. 4, p. 923–947, abr. 2005. Citado 4 vezes nas páginas 29, 33, 34, and 44.

RISKEN, H.; FRANK, T. *The Fokker-Planck Equation: Methods of Solution and Applications*. [S.l.]: Springer Science & Business Media, 2012. Citado na página 27.

SANCHO, J. M. et al. Analytical and numerical studies of multiplicative noise. *Phys. Rev. A*, American Physical Society, v. 26, n. 3, p. 1589–1609, set. 1982. Citado na página 34.

SANZENI, A.; HISTED, M. H.; BRUNEL, N. Emergence of irregular activity in networks of strongly coupled conductance-based neurons. *bioRxiv*, set. 2020. Citado na página 29.

SCHWALGER, T.; DROSTE, F.; LINDNER, B. Statistical structure of neural spiking under non-poissonian or other non-white stimulation. *J. Comput. Neurosci.*, v. 39, n. 1, p. 29–51, ago. 2015. Citado na página 29.

STANLEY, H. E. *Mean Field Theory of Magnetic Phase Transitions: Introduction to Phase Transitions and Critical Phenomena*. [S.l.]: Oxford University Press New York, 1971. Citado na página 19.

VOGELS, T. P.; RAJAN, K.; ABBOTT, L. F. F. Neural network dynamics. *Annu. Rev. Neurosci.*, v. 28, n. 1, p. 357–376, jan. 2005. Citado na página 19.

WEISS, P. L'hypothèse du champ moléculaire et la propriété ferromagnétique. *Journal de Physique Théorique et Appliquée*, Société Française de Physique, v. 6, n. 1, p. 661–690, 1907. Citado na página 19.

YEOMANS, J. M. *Statistical Mechanics of Phase Transitions*. [S.l.]: Clarendon Press, 1992. Citado na página 19.

YOSHIMURA, Y.; CALLAWAY, E. M. Fine-scale specificity of cortical networks depends on inhibitory cell type and connectivity. *Nat. Neurosci.*, v. 8, n. 11, p. 1552–1559, nov. 2005. Citado na página 19.

ZENKE, F.; AGNES, E. J.; GERSTNER, W. A diversity of synaptic plasticity mechanisms orchestrated to form and retrieve memories in spiking neural networks. *Nat. Commun.*, v. 6, n. 2011, p. 1–13, 2014. Citado na página 43.